Master's thesis

NTNU
Norwegian University of Science and Technology
Faculty of Medicine and Health Sciences
Department of Clinical and Molecular Medicine

Ingvild Lunde

Effects of doxorubicin on cell death and the transcriptome in human AC16 cardiomyocytes

Master's thesis in MSc in Molecular Medicine
Supervisor: Morten Høydal
Co-supervisor: Gurdeep Marwarha and Øystein Røsand
May 2022

NTNU
Kunnskap for en bedre verden

Ingvild Lunde

Effects of doxorubicin on cell death and the transcriptome in human AC16 cardiomyocytes

Master's thesis in MSc in Molecular Medicine
Supervisor: Morten Høydal
Co-supervisor: Gurdeep Marwarha and Øystein Røsand
May 2022

Norwegian University of Science and Technology
Faculty of Medicine and Health Sciences
Department of Clinical and Molecular Medicine

NTNU
Kunnskap for en bedre verden

Abstract

Background: Cancer and cardiovascular diseases are leading causes of death worldwide. Doxorubicin is a chemotherapeutic agent commonly used in cancer treatment; however, its use is limited by development of cardiotoxicity. Mechanisms involved in doxorubicin-induced cardiotoxicity include reactive oxygen species-induced oxidative stress and topoisomerase-2β inhibition, however the exact pathogenesis is not elucidated. Children are more susceptible to doxorubicin-induced cardiotoxicity than adults. Cardiotoxicity may cause heart failure, which in doxorubicin-treated patients have a mortality of nearly 50%. To develop preventive treatment strategies, it is necessary to increase the understanding of the processes involved in doxorubicin-induced cardiotoxicity. Therefore, the aims of this thesis were to (1) investigate the mechanisms of cell death induced by doxorubicin in AC16 cardiomyocytes, and (2) characterize the transcriptional changes in doxorubicin-treated AC16 cardiomyocytes.

Methods: AC16 cardiomyocytes were treated with doxorubicin (5μM) for 24 hours to assess the effect of the chemotherapeutic agent on cell death and transcription. Cell death was determined by lactate dehydrogenase assay, while cell viability and apoptosis were measured in a multiplexed assay. Transcriptional changes were explored through RNA sequencing, differential expression analysis, and gene set enrichment analysis.

Results: AC16 cardiomyocytes exposed to doxorubicin for 24 hours displayed significantly increased cell death and apoptosis, and significantly decreased cell viability ($p<0.0001$). A total of 17,013 differentially expressed genes were identified, of which 9,946 were upregulated and 7,067 were downregulated (FDR < 0.05). 13,042 differential expressed genes (p-value cut-off < 0.01) were forwarded to enrichment analysis. Enriched pathways and process networks were related to reactive oxygen species-induced oxidative stress, p53-dependent apoptosis, hypoxia, DNA damage responses and the developmental pathways of Wnt/βcatenin and Hedgehog. Differentially expressed genes involved in the DNA damage response were generally downregulated. The most relevant networks were mainly enriched in gene ontology processes related to embryonic development (Network 1), inflammation (Network 2), and cell growth (Network 3). Krüppel-like factor 4 appeared as a central hub in Network 1.

Conclusion: 24 hours of doxorubicin treatment increased cell death and apoptosis, and decreased cell viability in AC16 cardiomyocytes. Doxorubicin treatment induced transcriptional changes associated with apoptosis, oxidative stress, inflammation, downregulation of DNA damage response genes and reactivation of developmental pathways. The Krüppel-like factor 4, Yamanaka factors and Wnt/βcatenin-signalling appear as important in the doxorubicin-response. The novel observation of Hedgehog-signalling activation should be subject to further investigations.

Samandrag

Bakgrunn: Kreft og hjarte- og karsjukdom er leiande dødsårsaker i verda. Doxorubicin er mykje nytta som cellegift i kreftbehandling, men utvikling av kardiotoksisitet avgrensar bruken. Faktorar som bidreg til doxorubicin-indusert kardiotoksisitet inkluderer oksidativt stress indusert av reaktive oksygenforbindinger og hemming av topoisomerase-2β, men dei eksakte verknadsmekanismane er ikkje fullstendig klarlagt. Barn er meir sensitive for doxorubicin-indusert kardiotoksisitet enn vaksne. Kardiotoksisitet kan føre til hjartesvikt, som hjå pasientar behandla med doxorubicin har ei dødelegheit på nærare 50%. For å utvikle førebyggjande behandlingsstrategiar er det nødvendig å auke kunnskapen om prosessane involvert i doxorubicin-indusert kardiotoksisitet. Føremålet med denne oppgåva vart difor å (1) undersøke kva mekanismar som er involvert i doxorubicin-indusert celledød i AC16 kardiomyocyttar, og (2) beskrive endringar i transkriptomet til AC16 kardiomyocyttar som følgje av doxorubicin-behandling.

Metoder: AC16 kardiomyocyttar vart behandla med doxorubicin (5µM) i 24 timar for å vurdere kva effektar denne cellegifta har på celledød og transkripsjon. Celledød vart konstatert ved eit laktat-dehydrogenase-assay, medan celleviabilitet og apoptose vart bedømt ved bruk av eit kombinasjonsassay. Endringar i transkriptomet vart undersøkt ved hjelp av RNA-sekvensering, bioinformatikk og genuttrykksprofilering.

Resultat: AC16 kardiomyocytter eksponert for doxorubicin i 24 timar hadde signifikant auke i celledød og apoptose, og signifikant reduksjon i celleviabilitet ($p < 0.0001$). Totalt 17,013 gen var forskjellig uttrykt i dei to gruppene, der 9,946 var oppregulert og 7,067 var nedregulert (FDR < 0.05). 13,042 gen vart genutrykksprolifert. Dominerande signalvegar og prosessnettverk var relatert til oksidativt stress indusert av reaktive oksygenforbindinger, p53-avhengig apoptose, hypoksi, DNA-skaderesponsar og dei embryonale signalvegane Wnt/βcatenin og Hedgehog. Det var ei generell nedregulering av forskjellig uttrykte gen involvert i DNA-skaderesponsar. Dei mest relevante nettverka var assosiert med prosessar relatert til embryonal utvikling (Nettverk 1), inflammasjon (Nettverk 2) og cellevekst (Nettverk 3). Krüppel-like factor 4 framstod som ein hub i Nettverk 1.

Konklusjon: 24 timar med doxorubicin-behandling førte til auka celledød og apoptose, og redusert celleviabilitet i AC16 kardiomyocyttar. Doxorubicin behandling førte til endringar i transkriptomet relatert til apoptose, oksidativt stress, inflammasjon, nedregulering av gen involvert i DNA-skaderesponsen, og reaktivering av embryonale signalvegar. Krüppel-like factor 4, Yamanaka-faktorane og Wnt/βcatenin-signalering framstår som viktige i doxorubicin-responsen. Den hittil ukjende aktiveringa av Hedgehog-signalering bør utforskast vidare i framtidige studier.

Acknowledgements

This master thesis was carried out at the Department of Circulation and Medical Imaging, Faculty of Medicine and Health Sciences, Norwegian University of Science and Technology (NTNU) Trondheim. My supervisor through this project has been Professor and Head of Group of Molecular and Cellular Cardiology Morten Høydal and my co-supervisors have been Dr. Gurdeep Marwarha and Øystein Røsand.

The RNA library preparation, sequencing and bioinformatics analysis were performed in close collaboration with the Genomics Core Facility, NTNU. The Genomics Core Facility is funded by the Faculty of Medicine and Health Sciences at NTNU and Central Norway Regional Health Authority.

I could not have undertaken this work without my supervisor Morten. Thank you for giving me the opportunity to get to know this field of research, and for encouraging my independence while still always keeping your door open for questions and advice. I would also like to express my gratefulness to Nathan, Øystein and Gurdeep for always being available for assisting me in the lab, and for sharing your knowledge and experience. And thank you, Arnar, for providing support in the field of bioinformatics. I appreciate your patience and guidance. To all members of Group of Molecular and Cellular Cardiology, thank you for welcoming me to your team and for helping me whenever needed.

A special attention to the great people of Neufeldtsgate 18 for making my daily life in Trondheim a memorable time, to Sigri and Janne for being your caring and helpful selves, and to my family for always supporting me. Lastly, I would like to thank my dearest boyfriend Øystein for backing me through this process, by being my everyday motivational coach and comedian.

Table of Contents

List of Figures

List of Tables

Commonly Used Abbreviations

AP-1	Activator protein 1
ATM	Ataxia telangiectasia mutated
ATP	Adenosine triphosphate
ATR	Ataxia telangiectasia and Rad3 related
Bak	Bcl-2 Antagonist/Killer 1
Bax	Bcl-2 Associated X
Bcl	B-cell lymphoma
BH3	Bcl-2 homology domain 3
Brca1	Breast cancer-associated protein 1
CM	Cardiomyocyte
CVD	Cardiovascular diseases
DAMP	Damage associated molecular pattern
DDR	DNA damage response
DEG	Differential expressed gene
DMED	Dulbecco's Modified Eagle's Medium
DNA	Deoxyribonucleic acid
DOX	Doxorubicin
DR	Death receptor
DS	Double strand
EndMT	Endothelial mesenchymal transition
EV	Empty vector
FasR	Fas-receptor
FDR	False discovery rate
GO	Gene ontology
HIF	Hypoxia inducible factor
IL	Interleukin
KLF4	Krüppel-like factor 4
LDH	Lactate dehydrogenase assay
NCC	No-cell control
NFκB	Nuclear factor kappa B
PBS	Phosphate buffered saline
PCA	Principal component analysis
PRR	Pattern recognition receptor
RNA	Ribonucleic acid
ROS	Reactive oxygen species
TGF	Transforming growth factor
TLR	Toll like receptor
TNF	Tumour necrosis factor
TOP	Topoisomerase
TRAIL	TNF-related apoptosis-inducing ligand

1 Introduction

1.1 Cancer and Cardiovascular Diseases (CVDs)

Cancer and CVDs are leading causes of death and morbidity worldwide (1). According to the Cancer Registry of Norway[1], about 40% of the Norwegian population will develop cancer before the age of 80. Chemotherapeutics are commonly used in cancer treatment, targeting rapidly proliferating cells to prevent tumour growth. Doxorubicin (DOX) is an anthracycline that is widely used as a chemotherapeutic agent in the treatment of several cancer types, including breast cancer, gastrointestinal cancer, leukaemia, and lymphomas (2). Several anticancer effects of DOX have been described, including formation of DOX-DNA complexes that inhibits transcription and replication, generation of excessive reactive oxygen species (ROS) that cause oxidative damage, and inhibition of topoisomerase (TOP) 2α, a cell cycle enzyme that is overexpressed in most cancer cells (3). The common consequence of these mechanisms is subsequent induction of cell death in tumour cells. DOX has shown to be an effective chemotherapeutic agent; however, it also causes adverse effects on healthy tissue.

1.2 DOX-Induced Cardiotoxicity

The use of DOX in cancer treatment is limited by detrimental damage to healthy cardiac tissue (3). Cardiovascular side effects vary in severity and duration, and include arrythmias, inflammatory conditions, cardiomyopathies and heart failure (4). Terms regarding DOX-induced cardiotoxicity are not clearly defined (5). In this thesis the term DOX-induced cardiotoxicity will be used to describe the damage of cardiac tissue caused by DOX. Cardiomyopathy is a term used for several pathological conditions in the heart involving mechanical or electrical dysfunction, and ventricular hypertrophy or dilatation (6). The pathological decline in cardiac function caused by DOX-induced cardiotoxicity will therefore be referred to as DOX-induced cardiomyopathy.

[1] The Cancer Registry of Norway, Cancer in Norway 2020 - Cancer incidence, mortality, survival and prevalence in Norway, *Kreftregisteret*, Oslo, 2021, p.29, https://www.kreftregisteret.no/globalassets/cancer-in-norway/2020/cin-2020.pdf, (accessed 12.03.22).

Characteristics of DOX-induced cardiomyopathy is different between adults and younger patients. DOX-induced cardiomyopathy in adults is similar to dilated cardiomyopathy, while DOX-induced cardiomyopathy in juveniles is similar to restrictive cardiomyopathy (7). Common for both groups are the presence of systolic and diastolic dysfunction, and microscopical markers such as necrosis, fibrosis, loss of myofibrils and cardiomyocyte (CM) vacuolization (3, 5, 7). The onset of cardiotoxicity can be acute and cause symptoms within days or weeks after treatment, or it can manifest after several years (4). Prominent relationships have especially been characterized in children, where cancer survivors showed a 15-fold increased incidence of heart failure 30 years after receiving DOX treatment, compared to its siblings (4). DOX-induced cardiotoxicity also has an unquestionable dose-dependent relationship, with an incidence increasing from 5% with a dose of 400 mg/m^2 to 48% with a dose of 700 mg/m^2 (8). DOX-induced cardiomyopathy may eventually progress to congestive heart failure, which among DOX-treated patients has a mortality of nearly 50% after two years (9). This underpins the need for increased understanding of the pathogenesis involved in DOX-induced cardiotoxicity, in order to reduce mortality among cancer survivors.

1.3 Mechanisms of DOX-Induced Cardiotoxicity

Several mechanisms have been suggested to cause DOX-induced cardiotoxicity, including DNA intercalation, iron overload, inhibition of cardiac progenitor cells, and disturbed calcium homeostasis (3, 8, 10). However, the totality is complex and difficult to interpret (9). Nevertheless, two mechanisms stand out as major contributors to DOX-induced cardiotoxicity, namely increased oxidative stress, and inhibition of the cardiac specific isoform TOP2β (11, 12) (Figure 1).

Oxidative stress contribute to cardiotoxicity through generation of excessive ROS (13). The mitochondria have been extensively studied in this regard, due to their important functions in the highly metabolic heart. DOX accumulates in the mitochondria where it is thought to interfere with the electron transport chain, thereby disrupting energy production and increasing ROS generation (9). This cause opening of the mitochondrial permeability transition pore, resulting in

massive release of calcium into the cytosol. The intracellular homeostasis is consequently altered, thereby causing mitochondrial swelling, disruption of the mitochondrial membrane and subsequently cell death (14, 15). Since the mitochondria constitute over 30% of the CM volume and generate the vast majority of adenosine triphosphate (ATP) produced in the heart (14), these alterations are detrimental to cardiac function (9).

The initial purpose of DOX is to induce apoptosis in cancer cells, amongst others through TOP2α-inhibition which induce double stranded (DS) DNA breaks (9). Recent findings suggest that DOX also binds to the cardiac specific TOP2β in CMs, exerting the same mechanisms in healthy cardiac tissue (10, 12). DOX forms a complex with DNA and TOP2β and thereby induces DS DNA breaks (8, 11). Further, this is believed to cause the cascade of events associated with DOX-induced cardiotoxicity (11, 16).

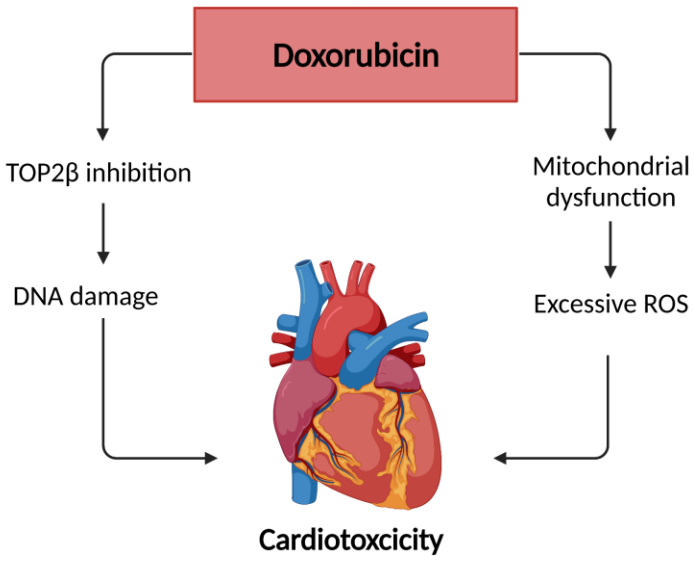

Figure 1: Mechanisms of DOX-induced cardiotoxicity

Simplified illustration of the current distinctive mechanisms believed to cause DOX-induced cardiotoxicity. DOX accumulates in the mitochondria where it interferes with the electron transport chain and cause generation of excessive ROS. This induce opening of the mitochondrial permeability transition pore, calcium overload, mitochondrial swelling and eventually cell death (14, 15). TOP2β-inhibition cause DNA damage in CMs, thereby inducing a cascade of events leading to cardiotoxicity. The figure was created with BioRender.com. CM: Cardiomyocyte, DNA: Deoxyribonucleic acid, DOX: Doxorubicin, ROS: Reactive oxygen species, TOP2β: Topoisomerase 2β.

1.4 DNA Damage Response (DDR)

It is evident that DOX induce genotoxic stress and DNA damage (3, 9), and the common consequence of DNA breaks is the activation of DDR (17). This involves formation of the MRE11-RAD50-NBS1 (MRN)-complex, and subsequent activation of Ataxia-telangiectasia mutated (ATM) and Ataxia-telangiectasia and Rad3-related (ATR) (Figure 2) (18). These checkpoint kinases mediate DNA break repair, cell cycle regulation and apoptosis through activation of signalling pathways and target genes. One important target gene is breast cancer-associated protein (BRCA) 1 which is central in homologous recombination of DS breaks (18, 19). ATM and ATR may also activate Activator Protein (AP-1), a transcriptional activator of genes involved in DNA repair and apoptosis, or Nuclear Factor kappa B (NFκB), mainly contributing to transcription of anti-apoptotic genes, thereby serving a pro-survival function (18, 20). NFκB and AP-1 is also involved in inflammatory processes, as will be discussed later.

Another central mediator activated in the DDR is the tumour suppressor p53. Upon DNA damage, p53 is stabilized and mediates its effects through transcriptional regulation of target genes. These genes are mainly involved in cell cycle arrest, DNA repair and apoptosis (3). Even though p53 has gained most attention regarding cancer development, recent findings suggests that p53's basal activity is necessary for normal cardiac homeostasis (21). Furthermore, elevated expression of this protein is observed in the progression of several CVDs including dilated cardiomyopathy and heart failure. P53 is thought to cause progression of these diseases through decreased angiogenesis, promotion of apoptosis and autophagy, and altered regulation of metabolism and cell cycle arrest (21). In response to chemotherapy-induced genotoxic stress, such as DOX, DNA damage induce activation of p53, which serves important roles in mediating the cell fate. However, the exact mechanisms of involvement in different cell types remains to be elucidated (17).

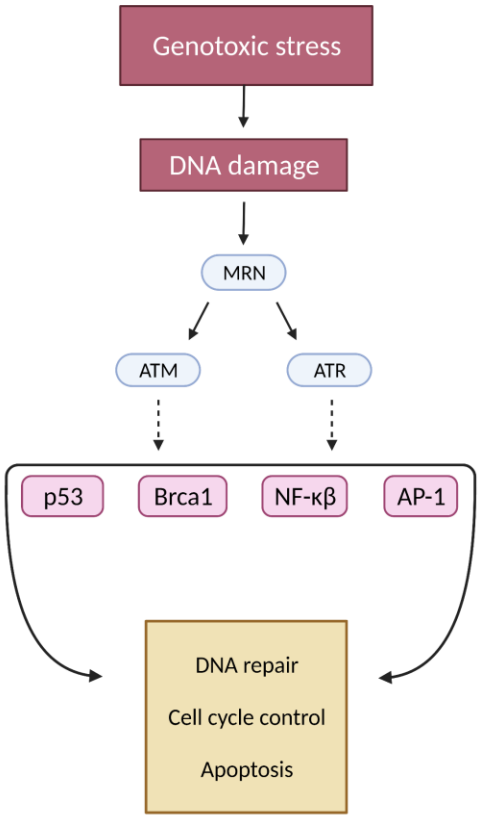

Figure 2: DNA damage response

Genotoxic stress induces DNA damage, thereby initiating the DDR through MRN-complex activation. Further, this complex activates ATM or ATR. This leads to activation of the transcription factors p53, Brca1, NFκB and AP-1. These transcription factors initiate transcription of genes involved in DNA repair, cell cycle regulation and apoptosis (19). The figure was created with BioRender.com. AP-1: Activator protein 1, ATM: Ataxia telangiectasia mutated, ATR: Ataxia telangiectasia and Rad3-related, Brca1: Breast cancer-associated protein 1, DDR: DNA damage response, DNA: Deoxyribonucleic acid, MRN: MRE11-RAD50-NBS1, NFκB: Nuclear factor kappa B.

1.5 Cell death, Senescence, and Inflammation in CVDs

While successful DNA repair leads to progression of the cell cycle, failed repair of severe DNA damage may induce cell death or senescence (Figure 3) (17). The main mechanisms of cell death associated with DOX-induced cardiotoxicity include necrosis, apoptosis, and autophagy (22). Apoptosis and autophagy are recognized as regulated and clean manners of cell death, involving timely degradation of dysfunctional cells, organelles, or proteins (23, 24). In contrast, necrosis is generally known as an unregulated and disordered cell death caused by physical or chemical cell damage (25).

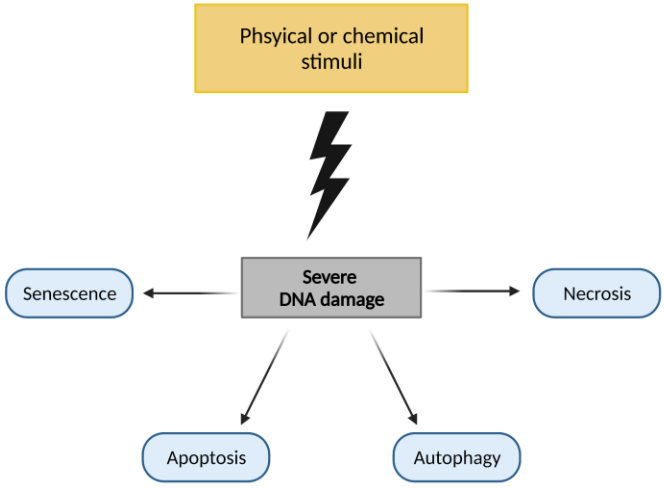

Figure 3: Consequences of unsuccessful DNA repair

DOX induce genotoxic stress and DNA damage to CMs. Severe DNA damage may induce different forms of cell death or senescence (17). The main mechanisms of cell death associated with DOX-induced cardiotoxicity includes apoptosis, necrosis and autophagy (22). The figure was created with BioRender.com. CM: cardiomyocyte, DNA: Deoxyribonucleic acid, DOX: Doxorubicin.

Heart failure is characterized by advancing dysfunction and death of CMs (25), and apoptosis has been suggested as a major contributor (26). There are two main pathways of apoptosis, namely the intrinsic and extrinsic (Figure 4). The intrinsic pathway (also known as the mitochondrial pathway) of apoptosis is initiated by a wide range of stimuli, including DNA damage, hypoxia, calcium-overload, and oxidative stress (27). This activates Bcl-2 homology domain 3 (BH3)-only proteins, which further activates the pro-apoptotic proteins Bcl-2 Associated X (Bax) and Bcl-2 Antagonist/Killer 1 (Bak). These proteins form pores in the outer mitochondrial membrane, thereby inducing release of cytochrome C into the cytosol. Cytochrome C and Apoptotic peptidase activating factor-1 (APAF-1) form the apoptosome, a complex that initiate apoptosis through activation of the caspase cascade (26). The final event is activation of the executioner caspases 3 and 7, which cause cell death through proteolysis of essential proteins (27).

Caspase 3 and 7 activation is also the final event in the extrinsic pathway (also known as the Death receptor (DR) pathway) of apoptosis. This pathway is activated by the binding of death signalling molecules to its respective receptors. Mediators previously described in cardiac tissue include Tumour necrosis factor (TNF) α , TNF-related apoptosis-inducing ligand (TRAIL) and Fas-

Ligand, and their respective receptors TNF Receptor 1, DR4/DR5 and Fas-receptor (FasR) (25). Interaction between the ligands and receptors initiates the cascade of events leading to caspase activation and apoptosis induction.

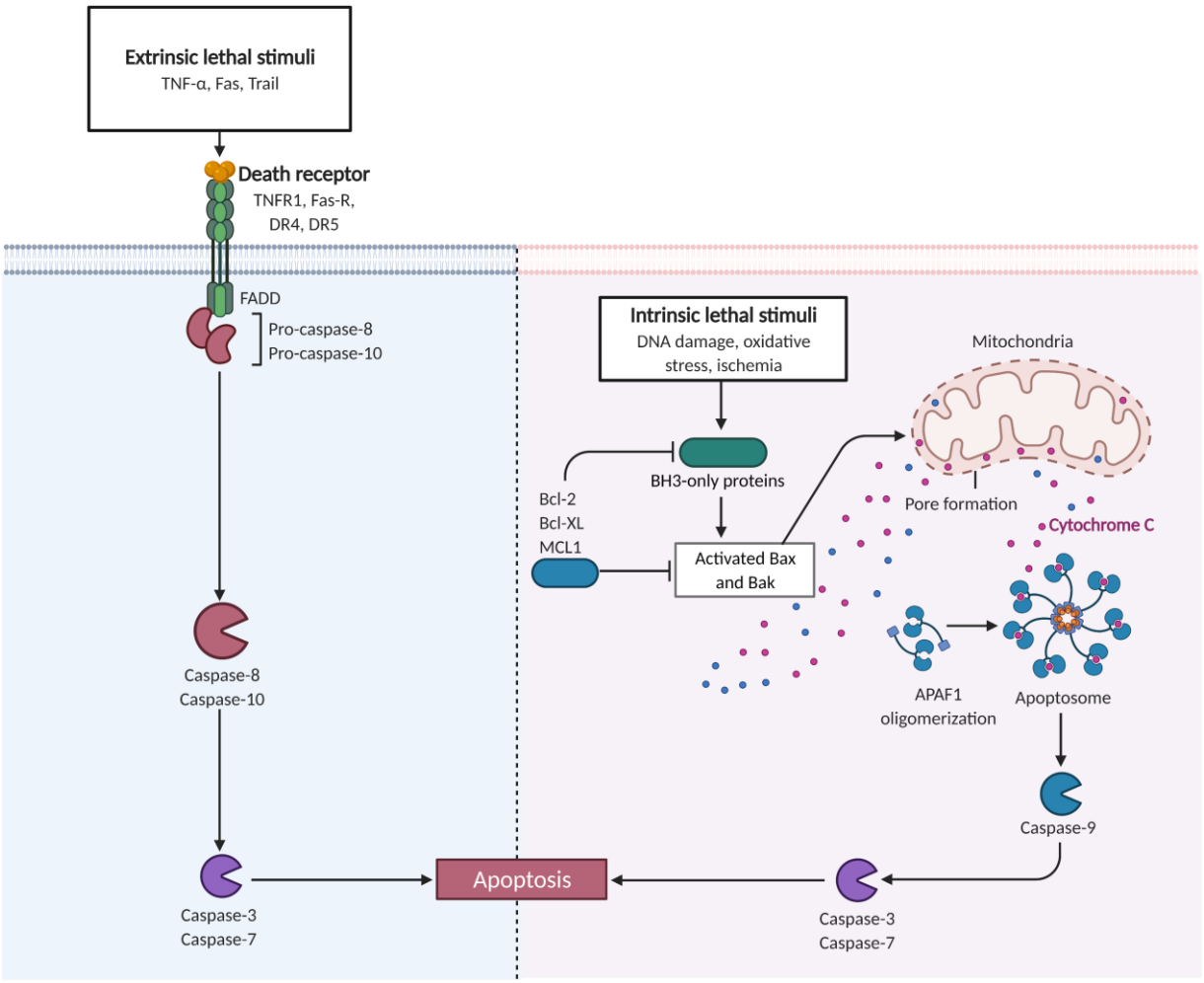

Figure 4: Extrinsic and intrinsic pathway of apoptosis

Simplified illustration of the extrinsic and intrinsic signalling pathways of apoptosis. External apoptotic stimuli, such as TNFα, Fas-ligand or TRAIL bind to its respective receptors, namely TNF Receptor 1, FasR, and DR4/DR5. This initiates a cascade of events leading to activation of the executioner caspases 3 and 7. These caspases induce apoptosis by proteolysis of essential proteins. Intrinsic apoptotic stimuli, such as DNA damage, oxidative stress or ischemia activates BH3-only proteins. These proteins further activate the pro-apoptotic mediators Bax and Bak, which initiates apoptosis through pore formation in the outer mitochondrial membrane, causing release of cytochrome C into cytosol (27). Cytochrome C and APAF-1 forms the apoptosome, a complex that initiates caspase activation and apoptosis. The figure is adapted from "Apoptosis Extrinsic and Intrinsic Pathways", by BioRender.com (2022). Retrieved from https://app.biorender.com/biorender-templates. APAF-1: Apoptotic peptidase activating factor-1, Bak: Bcl-2 Antagonist/Killer 1, Bax: Bcl-2 Associated X, BH3: Bcl-2 Homology 3, DNA: Deoxyribonucleic acid, DR: Death receptor, TNF: Tumour necrosis factor, TRAIL: Tumour necrosis factor-related apoptosis-inducing ligand, FasR: Fas-receptor.

As an alternative to apoptosis, damaged cells may also undergo senescence. This irreversible cell cycle arrest especially strikes post-mitotic cells, such as CMs (5, 24). Senescence can be part of normal physiology through telomere shortening, which is associated with normal aging processes (28). Alternatively, senescence can be induced by external stressors, such as oxidative stress or sustained DNA damage (29, 30), also known as stress-induced premature senescence (30). Senescence has been associated with several progressive CVDs, including cardiomyopathies, heart failure and DOX-induced cardiotoxicity (31). However, multiple aspects of senescence involvement in these diseases remain to be elucidated (31). Senescent cells can secrete characteristic signalling molecules such as pro-inflammatory cytokines and interleukins, then known as senescence-associated secretory phenotype (29). Secretion of these mediators will affect surrounding tissue and several of these factors are associated with cardiac fibrosis and inflammation (29).

Necrotic cell death also induce inflammation. CM disruption cause the release of intracellular damage associated molecular patterns (DAMPs). These are ligands for pattern recognition receptors (PRRs), of which there are several subtypes. Toll like receptor (TLR) 2 and TLR4 are the most extensively studied in the heart (32), and stimulation of these receptors initiates a cascade of events resulting in transcription factor activation. Two central transcription factors in inflammatory responses are NFκB and AP-1 (33). These transcription factors induce transcription of pro-inflammatory genes, including interleukin (IL)1, IL6, IL8 and TNFα, mediators that are also associated with cardiac dysfunction and pathology (32-35). Cardiac inflammation initiates tissue remodelling and fibrosis formation, and may eventually lead to development of heart failure (36). Due to their limited ability to divide, mature CMs are prone to such damaging inflammatory effects (25, 37).

Despite the severe side effects of DOX, this cytostatic drug is essential to overcome several malignancies and is therefore still broadly used in cancer treatment (3). This raises the need for development of treatment strategies that combat DOX-induced damage. Regeneration of cardiac tissue is emerging as a promising advancement in the treatment of cardiac injury (38). Such therapeutic agents would be an indispensable development to prevent DOX-induced cardiomyopathy.

This project therefore aimed to investigate the toxic effect of 24 hours of DOX treatment (5 μM) on AC16 CMs, an immortalized cell line derived from human cardiac ventricular tissue (39). Through cytotoxicity, cell viability and apoptosis assay we investigated the effect of DOX on cell death. Further, we explored the transcriptomic landscape changes caused by DOX treatment to potentially shed light on central pathways and processes contributing to cardiotoxicity. This led to the discovery of transcriptional alterations in processes related to apoptosis, oxidative stress responses, inflammation, the DDR, and development.

2 Aims and Hypothesis

To increase the understanding of DOX-induced cardiotoxicity the aims of this thesis were to:

1. Investigate the mechanisms of cell death induced by DOX in AC16 CMs.
2. Characterize the transcriptional changes in DOX-treated AC16 CMs.

The hypotheses underpinning these aims were:

1. DOX treatment induces acute cell death and apoptosis in AC16 CMs.
2. Transcriptome analysis and bioinformatics approaches can uncover central pathways, processes, and networks involved in DOX-induced cardiotoxicity, and thereby contribute to identification of novel therapeutic targets.

3 Materials and Methods

3.1 AC16 CMs and Maintenance

AC16 CMs (EMD Millipore, Billerica, MA, USA) were used in the following experiments. This is an immortalized cell line derived from ventricular tissue of human heart, that can proliferate in culture (39). This makes the cell line appropriate for use in experiments which require a significant amount of biological sample. Furthermore, the cell line possesses human genome and characteristic CM markers, making it suitable for studying physiological, pharmacological, and pathological effects of drugs on CMs (39).

AC16 CMs were cultured in pre-warmed culture medium, consisting of Dulbecco's Modified Eagle's Medium (DMED) (Thermo Fischer Scientific, Waltham, MA, USA), 12.5% Fetal Bovine Serum (Thermo Fischer Scientific, Waltham, MA, USA) and 1% Antibiotic Antimycotic Solution (Sigma Aldrich, Saint-Louis, MO, USA), and maintained in a humidified incubator with 5% CO_2 at 37 ˚C. Splitting ratio and frequency depended on confluency and experimental requirements.

The subculturing procedure was performed as follows. Culture medium was aspirated, and 4 ml Trypsin (Thermo Fisher Scientific, Waltham, MA, USA) was added to the cells followed by incubation at 37 ˚C for 3-4 min. Culture medium was added 1:1 to terminate trypsinization. Trypsin was removed by centrifugation of the suspension at 300 x *g* for 3 min followed by removal of the supernatant. Cells were then resuspended in culture medium and seeded onto 100 mm culture plates (BioLite 100mm tissue culture dish, Thermo Fisher Scientific, MA, USA) containing culture medium. Cells with passage number up to 10 was used in the experiments. Experiments were performed in either 100 mm culture plates (Lactate dehydrogenase (LDH) assay and RNA isolation) or a 96-well plate (Multiplexed cell viability and apoptosis assay) (Figure 5).

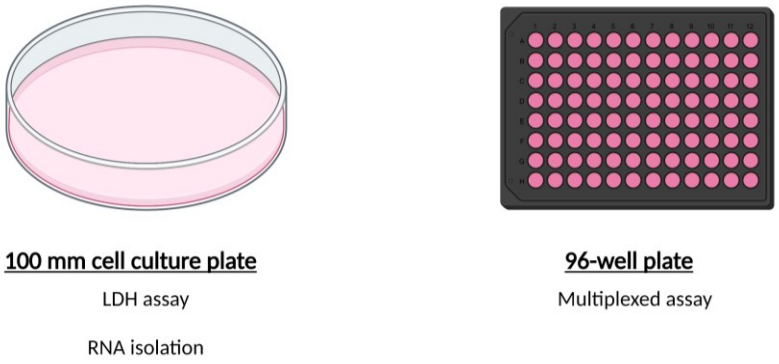

Figure 5: Cell culture experiment outline

Basic outline of the cell culture experiments. AC16 CMs were seeded in 100 mm cell culture plates prior to LDH assay and RNA isolation, and in a 96-well plate prior to the multiplexed assay. The figure was created with BioRender.com. DOX: Doxorubicin, LDH: Lactate dehydrogenase, RNA: Ribonucleic acid.

3.2 Transfection

Due to unexpected circumstances the direction of the project had to be changed. The original project aimed to investigate the protective effect of a specific protein on AC16 CMs. Cells were therefore transfected with either protein overexpression vector or empty vector (EV) prior to assay and RNA sequencing. Limitations in time and costs did not allow repetition of these experiments on non-transfected cells. Therefore, cells used in this project are transfected with EV.

Cells were forward transfected with empty vector (EV) provided by Dr. Akira Sawa at the Department of Psychiatry, Johns Hopkins University School of Medicine, USA. At the time of transfection, the plates were approximately 80% confluent. EV plasmid had a concentration of 1 µg/µl. The transfection mix ratio was 1:5:50 for plasmid, transfection reagent and medium, respectively. For one 100 mm plate of cells, we used 3 µg of plasmid resulting in 36 µl of each plasmid group solution for 12 plates. EV plasmid was added to a 1.5 ml tube containing plain DMED, and incubated in room temperature for 5 min. Further, Polyfect Transfection Reagent (Qiagen, Hilden, Germany) was added to the medium, followed by incubation at 37 ˚C for 30 min. The transfection mix was then added to cell culture medium holding 37 ˚C, and 10 ml of this solution was distributed to each of the plates. Plates containing the transfection mix incubated

at 37 ˚C for approximately 7 hrs. Transfection medium was then replaced by culture medium, followed by incubation at 37 ˚C for 14 hrs to let the cells recover from transfection.

3.3 DOX Treatment

To assess the effect of the chemotherapeutic agent on AC16 CMs, cells were treated with 5 µM DOX (Sigma Aldrich, Saint Louis, MO, USA) for 24 hrs. The chosen DOX concentration and treatment duration was based on findings by Berg et.al (40). The treatment duration was further determined by a pilot study comparing LDH activity between 12 hrs and 24 hrs of DOX treatment (Appendix I).

Following transfection, cells were treated with either DOX-containing medium (5 µM) or vehicle medium (sterile water) (B. Braun, Melsungen, Germany). First, DOX was dissolved in sterile water to achieve a stock solution concentration of 1 mM. Further, DOX was diluted in culture medium to achieve a final concentration of 5 µM. Four plates were treated with 10 ml DOX-containing medium and 10 ml vehicle medium, respectively, giving four technical replicates and two biological replicates. All plates were incubated at 37 ˚C for 24 hrs. No-cell controls (NCCs), containing culture medium and either DOX or sterile water, were treated the same way and used as blanks in the LDH assay.

3.4 LDH Assay

An LDH assay was performed to determine the level of cell death induced by DOX. The LDH assay allows fast and reliable detection of cytotoxicity in cell culture (41). Upon cell membrane disruption, cytoplasmic LDH is released into the culture medium, thereby indicating cell damage and death (42).

Cells were transfected and treated with DOX as described in sections 3.2 and 3.3, followed by LDH activity measurements using the Cytotox 96® Non-Radioactive Assay kit (Promega, Madison, WI, USA) (Figure 6). First, condition medium was collected from all plates. Then, 1 ml of RIPA

buffer (Santa Cruz Biotechnology, Dallas, TX, USA) containing 10 µl Halt™ Protease Inhibitor Cocktail (Thermo Fischer Scientific, Waltham, MA, USA) and 10 µl Halt™ Phosphatase Inhibitor Cocktail (Thermo Fischer Scientific, Waltham, MA, USA) was added to the plates immediately after removing the medium to induce cell lysis. Cells were stored at 4 ˚C and harvested after 3 hrs. Condition medium was diluted 1:5 by adding 200 µl of condition medium into 800 µl of Phosphate buffered saline (PBS) (EMD Millipore, Billerica, MA, USA). NCCs, only containing culture medium, was diluted the same way. 50 µL of the diluted condition medium and NCCs were then seeded onto a 96-well plate (VWR® Tissue Culture Plates, VWR International, Radnor, PA, USA) in triplicates. 50 µL Substrate mix dissolved in 12 ml of Assay buffer was added to each well, followed by incubation in room temperature for 40 min, protected from light. Then, 50 µL Stop Solution from the assay kit was added to each well. The plate was immediately read at 490 nm using FLUOstar Omega microplate reader (BMG LABTECH, Offenburg, Germany).

3.5 RNA Isolation

To assess the transcriptional changes caused by DOX, total RNA was isolated from the AC16 CMs after 24 hrs of DOX treatment. Transfection and DOX treatment was performed as described in sections 3.2 and 3.3, followed by RNA isolation using the miRNeasy Mini Kit (Qiagen, Hilden, Germany) (Figure 6). Condition medium was removed from each plate, followed by addition of 1,200 µL Qiazol (Qiagen, Hilden, Germany) to the cells. Cell lysate was collected and vortexed to ensure lysis, followed by incubation in room temperature for 5 min. Cell lysate from each technical replicate was divided into two separate tubes and stored at -80 ˚C.

Cell lysates were thawed in room temperature, before addition of 120 µL Chloroform (Sigma Aldrich, Saint Louis, MO, USA) to the samples. The content was then mixed by shaking the tube by hand for 30 sec. The mixed cell lysates were then incubated for 15 min at room temperature, while shaking every 5 min, followed by centrifugation at 12,000 x *g* for 20 min at 4 ˚C. After centrifugation, the aqueous phase (350 µL) was transferred to a collection tube. Then, Absolute alcohol prima (Antibac, Asker, Norway) was added in a 1:2 ratio, followed by thorough mixing by pipetting. 500 µL of the sample was added to and RNeasy Mini spin column, placed in a 1.5 ml

collection tube and centrifuged at 8,100 x *g* for 1 min at room temperature. The flow through was discarded, and the step was repeated with the remaining sample.

The new flow through was discarded and 500 µL RPE buffer was added to the spin column, followed by centrifugation for 1 min at 8,100 x *g* at room temperature. This step was repeated and followed by centrifugation for 5 min to dry the column membrane. The spin column was then transferred to a new 1.5 ml tube and 50 µL of RNase-free water was added directly to the centre of the column membrane, followed by incubation for 5 min. Finally, the samples were centrifuged at 8100 x *g* for 5 min at room temperature. RNA concentration and purity control was measured using Nano Drop 2000 spectrophotometer (Thermo Fischer Scientific, Waltham, MA, USA) at the ratios 260/230 and 260/280 (Appendix II). Pure RNA (260/230 and 260/280 ratio ~ 2.0) from both experimental groups were forwarded to RNA sequencing.

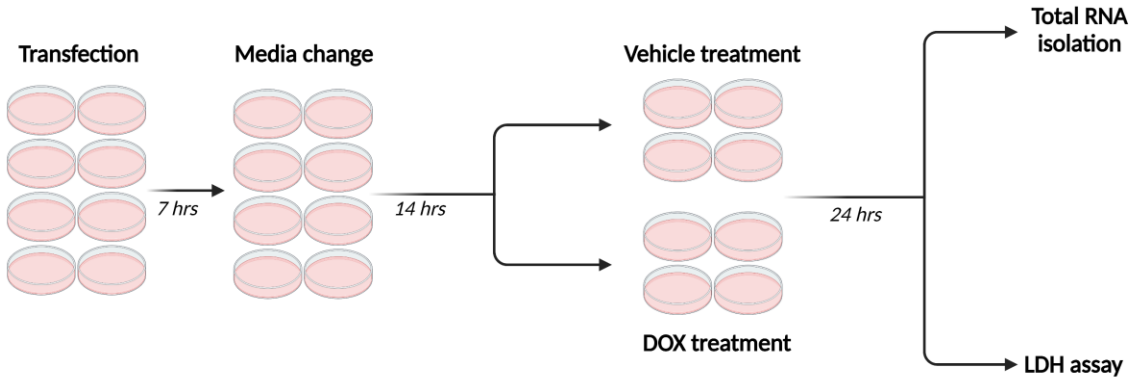

Figure 6: Experimental setup for the LDH assay and RNA isolation

Prior to LDH assay and total RNA isolation, cells were seeded in eight 100 mm plates and transfected with EV. Further, four plates were treated with either sterile water or DOX. For the LDH assay, NCCs containing only culture medium and sterile water, or culture medium and DOX was treated the same way (not shown). The figure was created with BioRender.com. DOX: Doxorubicin, LDH: Lactate dehydrogenase, NCC: No-cell control, RNA: Ribonucleic acid.

3.6 Cell Viability and Apoptosis Assay

The mechanism of cell death was assessed by ApoLive-Glo™ Multiplex Assay (Promega, Madison, WI, USA), performing simultaneous detection of cell viability and apoptosis. Obtaining different measurements from the same sample will reduce errors related to environmental and treatment conditions, thereby providing more reliable results. Viability was measured by live-cell protease

activity and apoptosis was measured by caspase 3/7 activity. Compared to alternative viability assays such as resazurin, live-protease activity shows little toxic effects, making it suitable for multiplexing (43).

Cells were counted using Countess II Automated Cell Counter (Thermo Fisher Scientific, Waltham, MA, USA) and seeded in a 96-well plate at a density of 10,000 cells/well. The outer wells contained PBS to avoid evaporation, thereby reducing the edge-effect. Transfection and treatment protocol was implemented as described in sections 3.2 and 3.3, however, with minor changes concerning recovery time after seeding and transfection (Figure 7). These changes were as follows: 12 hrs after seeding, cells were forward transfected. A transfection master mix containing 9 µl (1 µg/µL) vector, 45 µL transfection reagent and 450 µl medium was made as previously outlined. 12.6 µl of the transfection mix was subsequently added to 6 ml of prewarmed culture medium. Further, 200 µl of transfection medium was added to each well, resulting in 7.5 ng of vector in each well. After 7 hrs, transfection medium was replaced by 200 µl culture medium to let the cells recover from transfection for 16 hrs. After recovery, cells were treated with either DOX containing medium or vehicle medium for 24 hrs.

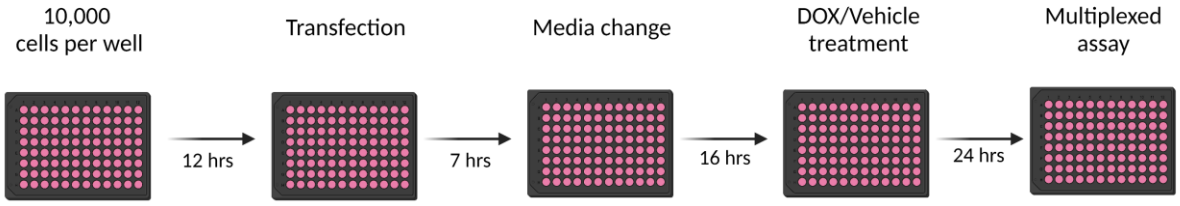

Figure 7: Experimental setup for the multiplexed assay

Workflow prior to the multiplexed cell viability and apoptosis assay. Cells were seeded at a density of 10,000 cells per well, and forward transfected after 12 hrs. Cells were exposed to transfection medium (7 ng per well) for 7 hours. Then, transfection medium was replaced by culture medium to let the cells recover from transfection. After 16 hours of recovery, cells were treated with DOX containing medium (5µM) or vehicle medium (sterile water) before performing the multiplexed cell viability and apoptosis assay. The figure was created with BioRender.com. DOX: Doxorubicin.

There were four biological replicates in each of the experimental groups, and three technical replicates for each biological sample (Figure 8). There were also two triplicates of NCCs used as

blanks, containing DOX medium and vehicle medium, respectively. Following treatment, the multiplexed assay was performed. The viability reagent was made by adding 10 µl of substrate to 2 ml of assay buffer, both obtained from the ApoLive-Glo™ Multiplex Assay kit. 20 µl of viability reagent was added to all wells. This was mixed by orbital shaking at approximately 400 rpm for 30 sec, followed by incubation at 37 ˚C for 1.5 hrs. Fluorescence was then measured at 400Ex/505Em. 100 µl Caspase-Glo® 3/7 Reagent was then added to all wells, followed by incubation for 1.5 hrs at room temperature hidden from light. Finally, luminescence was measured at 1 sec exposure.

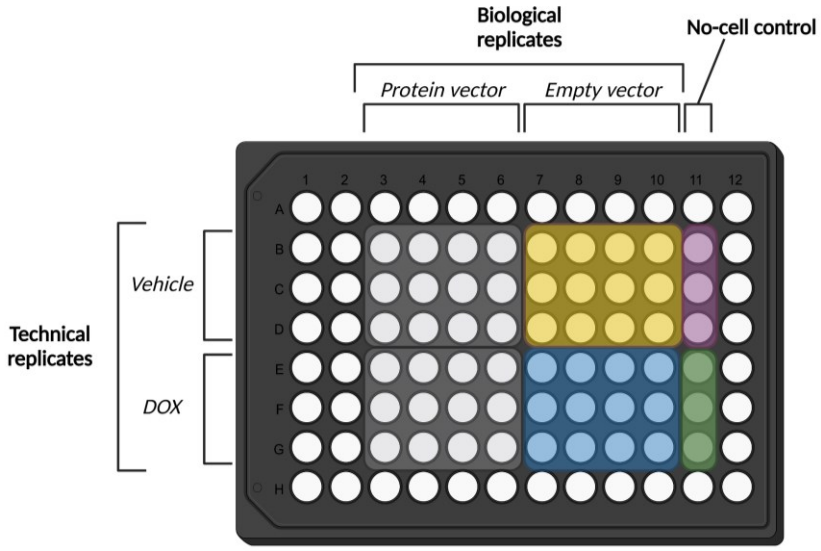

Figure 8: 96-well plate outline for the multiplexed assay

Cells were seeded at a density of 10,000 cells per well. The outer wells (white) contained PBS to avoid evaporation, thereby reducing the edge-effect. The 96-well plate contained four experimental groups, however, only results from EV vehicle-treated (yellow) and EV DOX-treated (blue) are reported in this project. There were four biological replicates in each experimental group, and three technical replicates for each biological sample. NCC vehicle-treated (purple) and NCC DOX-treated (green) were used as blanks in the assay. The figure was created with BioRender.com. DOX: Doxorubicin, EV: Empty vector, NCC: No-cell control, PBS: Phosphate buffered saline.

3.7 RNA Sequencing and Data Analysis

Isolated RNA was sequenced and analysed by the Genomics Core Facility at NTNU. Compared to hybridization-based methods, RNA sequencing is not dependent on prior knowledge of the generated sequences and shows higher sensitivity. This allows for reliable identification of known and novel transcripts, that further can be used in functional analysis.

3.7.1 Library Construction and Sequencing

Total RNA was isolated as described in section 3.5. Additional RNA concentration and purity control was performed by the Genomics Core Facility at NTNU. RNA concentration was measured using Qubit® RNA HS Assay Kit on a Qubit® 3.0 Fluorometer (Thermo Fisher Scientific, Waltham, MA, USA). Integrity was assessed using Agilent RNA 6000 Nano Kit on a 2100 Bioanalyzer instrument (Agilent Technologies, Santa Clara, CA, USA).

RNA sequencing libraries were prepared using the Illumina Stranded mRNA prep ligation kit (Illumina, San Diego, CA, USA) according to the manufacturer's instructions. An overview of the library construction process is illustrated in Figure 9. In brief, 875 ng total RNA was used as starting material. First, mRNA was purified from the total RNA by using poly-T oligonucleotide-attached magnetic beads, followed by random fragmentation at 94°C for 8 min. First strand cDNAs were synthesized by reverse transcription, using random hexamer oligonucleotides. This includes Actinomycin D, which allows RNA-dependent synthesis and improves strand specificity while preventing spurious DNA-dependent synthesis. Then, the RNA template is removed, followed by synthesis of the second cDNA strand, where dTTP is replaced by dUTP to quench the second strand during amplification and achieve strand specificity. Further, double stranded cDNA is blunted and adenylated at the 3'-prime ends. Adaptors required for sequencing are ligated to the cDNA. These contain primer binding sites and unique dual index adapter oligonucleotides, respectively.

Libraries were purified using the AMPure XP (Beckman Coulter, Inc., Indianapolis, IN, USA), and subjected to 11 cycles of PCR amplification. An additional purification step was performed using the AMPure XP (Beckman Coulter, Inc., Indianapolis, IN, USA), followed by quantification by qPCR using KAPA Library Quantification Kit (Kapa Biosystems, Inc., Wilmington, MA, USA) and validation using Agilent High Sensitivity DNA Kit on a Bioanalyzer (Agilent Technologies, Santa Clara, CA, USA). The size of the DNA fragments was measured to be in the range of 200-1000 base pairs and peaked around 274 base pairs.

Indexed libraries were normalized and pooled to 2.6 pM and subjected to clustering on a NextSeq 500 high output flow-cell (Illumina, San Diego, CA, USA). Finally single read sequencing was

performed for 72 cycles on a NextSeq 500 instrument (Illumina, Inc. San Diego, CA, USA), according to the manufacturer's instructions. Base calling was done on the NextSeq 500 instrument by RTA 2.4.6. FASTQ files were generated using bcl2fastq2 Conversion Software v2.20.0.422 (Illumina, Inc. San Diego, CA, USA).

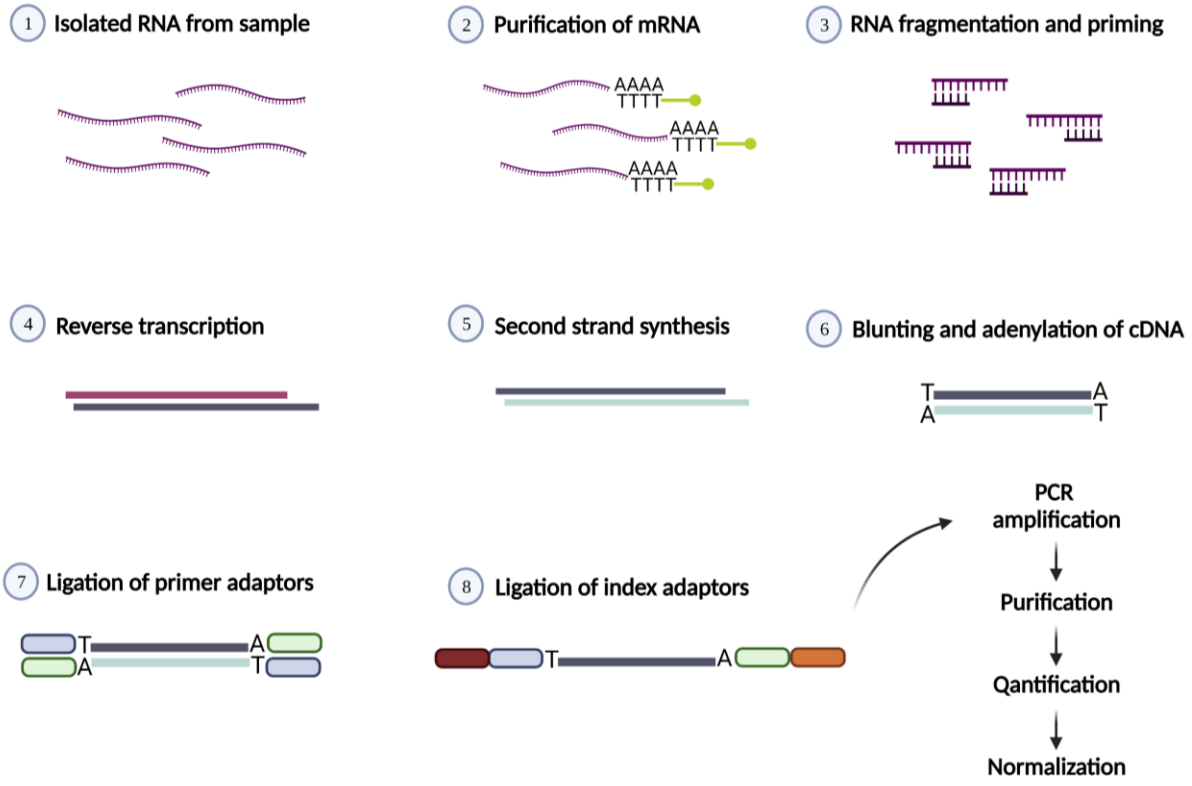

Figure 9: Library construction

Simplified illustration of the library construction process [2]. Isolated RNA from DOX and vehicle-treated samples were first purified by polyA-tail-selection using poly-T oligonucleotide-attached magnetic beads. Then, RNA was fragmented to achieve bp lengths appropriate for RNA sequencing (200-1,000 bp). Primers were added, and mRNA was reverse transcribed, giving the first strand of cDNA. The second strand was then synthesized, followed by blunting of the cDNA and adenylation of the 3'-end of the strands. Adaptors containing primer binding sites and unique dual index adapter oligonucleotides were ligated to the cDNA. Finally, cDNA was amplified by 11 cycles of PCR, purified, quantified, and normalized, before the prepared indexed libraries were forwarded to sequencing. The figure was created with BioRender.com. Bp: Base pair, cDNA: complementary DNA, DNA: Deoxyribonucleic acid, DOX: Doxorubicin, mRNA: Messenger RNA, PCR: Polymerase chain reaction, RNA: Ribonucleic acid.

[2] The figure was adapted from Illumina Stranded mRNA Data Sheet: https://www.illumina.com/content/dam/illumina-marketing/documents/products/datasheets/illumina-stranded-mrna-data-sheet-470-2020-002.pdf, (accessed 14.04.22)

3.7.2 Data Analysis

After RNA sequencing, FASTQ files were filtered and trimmed (fastp v0.20.0) and transcript counts were generated using quasi alignment (Salmon v1.3.0) to the transcriptome reference sequence (Ensembl, GRCh38 release92). Transcript sequences were imported into the R statistical software and aggregated to gene counts using the tximport (v1.14.0) Bioconductor package (44). Gene counts were normalized to the vehicle-treated group and analysed for differential expression using the DESeq2 Bioconductor package (45, 46). DESeq2 is a specialized software for analysis of RNA-sequencing data and builds a generalized linear model under the assumption of negative binomial distributed values and uses the Wald statistic for significance testing. Benjamin Hochberg P-value adjustment was performed to account for multiple testing (FDR < 0.05).

3.8 Gene Set Enrichment Analysis

Following data processing (summarized in figure 10), gene set enrichment analysis was performed using the *Analyze Single Experiment Workflow* in Metacore™ (Version 22.1, Clarivate ©2022). Metacore is a bioinformatics database software, where validated and peer reviewed literature forms the basis for the functional analysis. The enrichment analysis allows for identification of relevant pathways, processes, networks, and diseases in the uploaded gene set. Enriched diseases are not reported in this project, and GO processes are only reported regarding the network analysis. Only differentially expressed genes (DEGs) with p-value cut-off < 0.01 was included in the enrichment analysis. The expression threshold value was set to default.

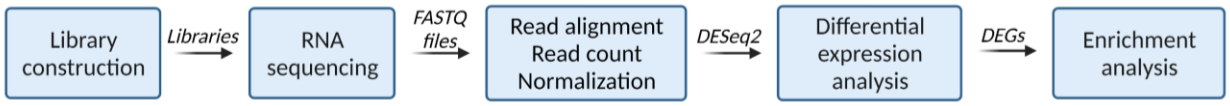

Figure 10: Bioinformatics workflow

Overview of the bioinformatics workflow following library construction of mRNA isolated from DOX- and vehicle-treated AC16 CMs. Prepared libraries were forwarded to RNA sequencing. Generated FASTQ files from RNA sequencing were aligned, counted, and normalized, before they were forwarded to differential expression analysis, using the DESeq2 software. Identified DEGs were then subjected to gene set enrichment analysis. The figure was created with BioRender.com. CM: Cardiomyocyte, DEG: Differential expressed gene. DOX: Doxorubicin, RNA: Ribonucleic acid.

The enrichment analysis match gene IDs from the uploaded gene set with gene IDs in already existing Metacore functional ontologies (canonical pathway maps, process networks, GO processes and diseases). The given p-value for the enriched pathways, networks and processes is based on hypergeometric distribution to adjust for different object numbers in the entire database, the uploaded gene set, and the Metacore pathways, processes, and networks [3]. The *Analyze Single Experiment Workflow* also calculates unique networks for the uploaded gene set, based on interactions between objects in the uploaded gene set and objects in the Metacore database, presence of canonical pathway fragments and enrichment in GO processes. The statistical basis for the enrichment and network analysis is illustrated in figure 11.

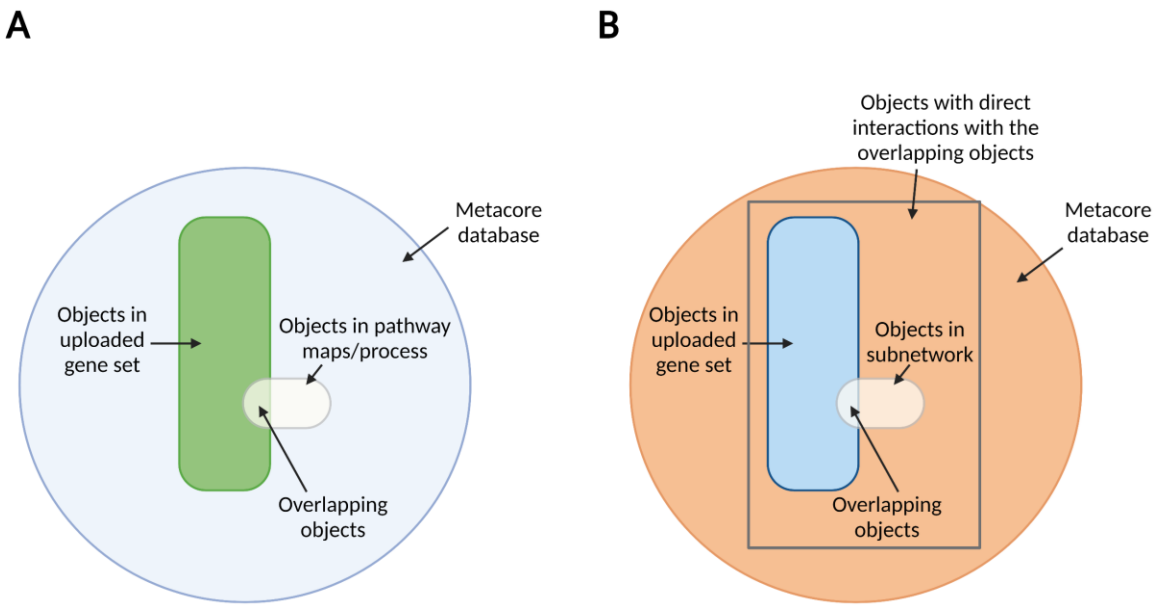

Figure 11: The statistical basis for the enrichment and network analysis

*Simplified illustration of the statistical basis for the enrichment analysis **(A)** and network analysis **(B)** [4]. The given p-value for the enriched pathways, processes and networks is based on hypergeometric distribution to adjust for different object numbers in the uploaded gene set, pathways/processes/subnetworks, and the entire database. The network analysis also accounts for objects in the Metacore database with direct interactions with the overlapping objects, presence of canonical pathway fragments and enrichment in GO processes. The figure was created with BioRender.com. GO: Gene ontology.*

[3] Background theory for the enrichment analysis was derived from GeneGo's Metacore online support: https://portal.genego.com/help2/wwhelp/wwhimpl/js/html/wwhelp.htm#context=metacore&topic=mc_overview , (accessed 15.02.22).

[4] The figure was adapted from GeneGo's Metacore online support (Understanding Enrichment Analysis Statistics): https://portal.genego.com/help2/wwhelp/wwhimpl/js/html/wwhelp.htm#context=metacore&topic=mc_overview , (accessed 02.04.22).

3.9 Statistical Analysis

Statistical analyses of the cytotoxicity, apoptosis and cell viability assay were performed using GraphPad Prism (Version 9.2.0 for Windows, GraphPad Software, San Diego, California USA, www.graphpad.com). An unpaired Student`s t-test was conducted to determine the statistical value of the results. Data is presented as mean with standard deviation. We considered p-values below 0.05 significant for these analyses.

4 Results

4.1 Cell Death Analysis in AC16 CMs

Mechanisms of cell death induced by DOX was investigated by cytotoxicity, cell viability and apoptosis assays. Assays showed a significantly higher cell death and lower cell viability in DOX-treated CMs. We found a significant increase in LDH activity in the DOX-treated group (0.99 ± 0.43) compared to the vehicle-treated group (0.18 ± 0.02) ($p < 0.0001$) (Figure 12A). The observed differences in cell death were further explored in a multiplexed apoptosis and cell viability assay. We found a significant difference in live-cell protease activity between the DOX-treated (1.13 ± 0.10) and vehicle-treated groups (3.28 ± 0.40) ($p = < 0.0001$) (Figure 12B). The same was seen for apoptosis, where the DOX-treated (4.18 ± 0.26) and vehicle-treated (1.10 ± 0.12) groups had a significant difference in Caspase 3/7-activity ($p < 0.0001$) (Figure 12C).

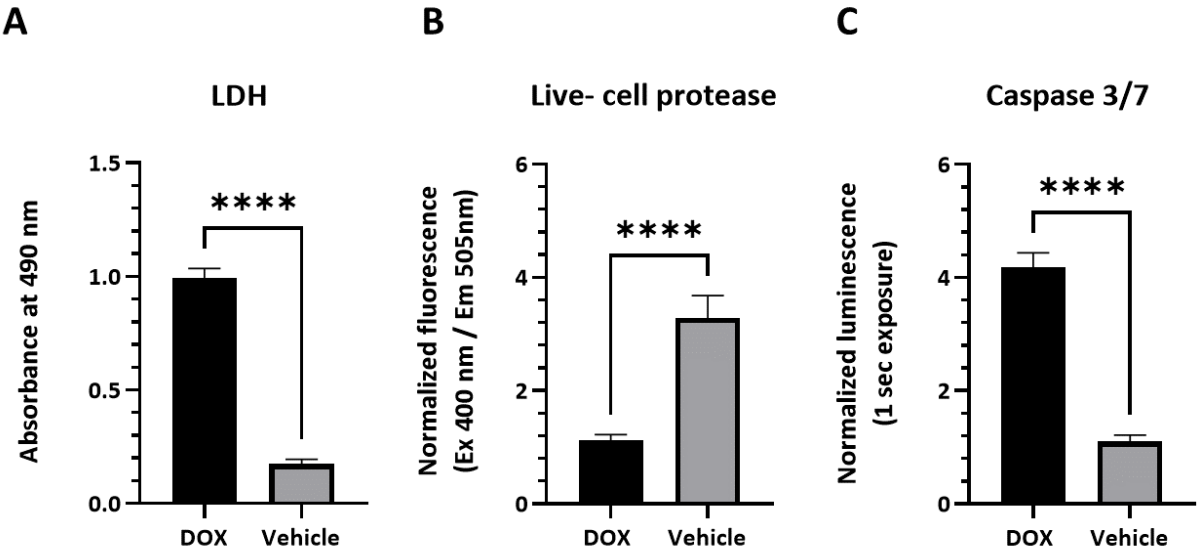

Figure 12: Effect of DOX on AC16 CMs

*LDH activity **(A)**, live-cell protease activity **(B)** and caspase 3/7-activity **(C)** results for AC16 CMs exposed to DOX (5 µM) and sterile water for 24 hours. Absorbance was measured at 490 nanometres for the LDH assay, fluorescence was measured at 400 nanometres excitation and 505 nanometres emission, and luminescence was measured at 1 second exposure. Data are presented as mean with standard deviation. p<0.0001 = ****. DOX: Doxorubicin, Em: Emission, Ex: Excitation, LDH: Lactate dehydrogenase.*

4.2 Variability and Differential Expression Analysis

Differential expression analysis was performed to assess the transcriptional changes caused by DOX. PC1 (90,78%), illustrated in Figure 13A, shows clear separation between and clustering within the two biological groups, giving evidence for consistent variability between DOX-treated and vehicle-treated AC16 CMs. A total of 49,910 genes were aligned during data processing (data not shown), and differential expression analysis identified a total of 17,013 DEGs, of which 9,946 were upregulated and 7,067 were downregulated (FDR < 0.05) (Figure 13B).

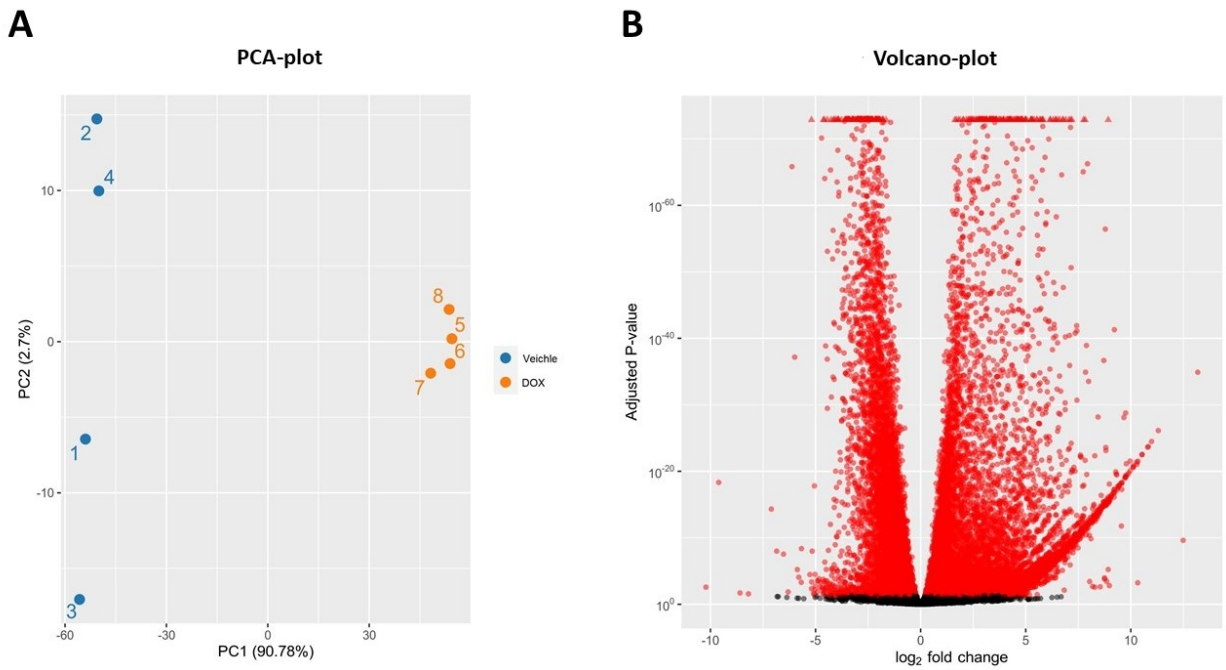

Figure 13: PCA plot and Volcano plot

(A) *The variability in the gene set is visualized in the PCA plot. PC1 (90,78%) separates samples according to biological condition, showing significant differences between DOX and vehicle-treated samples. Blue dots (1-4) represent vehicle-treated samples, while orange dots (5-8) represent DOX-treated samples.* ***(B)*** *Differential expression analysis revealed a total of 17,013 statistically significant DEGs, where 9,946 were upregulated and 7,067 were downregulated (FDR < 0.05). The Y-axis represent the statistical significance (adjusted p-value) and the X-axis represent the log2FC of DEGs in the two experimental conditions. DEGs with negative and positive log2FC are downregulated and upregulated, respectively. One dot represents one DEG. Red dots are significant (FDR < 0.05), while black dots are not significant. DEG: Differentially expressed gene, DOX: Doxorubicin, FC: Fold change, FDR: False discovery rate, PCA: Principal component analysis.*

4.3 Enrichment Analysis – Pathways and Process Networks

An enrichment analysis was performed to explore the biological changes associated with the identified DEGs. A total of 13,042 DEGs were included in the analysis after p-value cut-off < 0.01 (Figure 14). DEGs are reported with Metacore annotations.

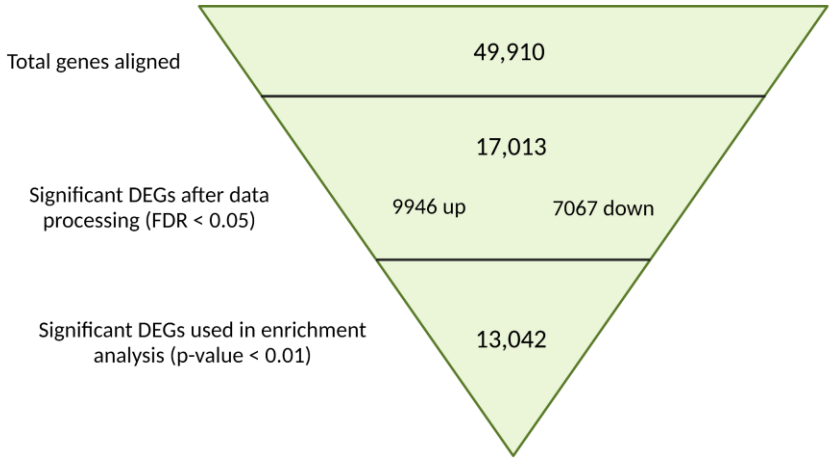

Figure 14: Gradual reduction of DEGs from RNA sequencing to enrichment analysis

The gradual reduction of genes during differential expression analysis and prior to enrichment analysis. A total of 49,910 genes was aligned during RNA sequencing. 17,013 genes were included after differential expression analysis (FDR < 0.05). P-value cut-off < 0.01 was set prior to the enrichment analysis. The figure is inspired by McSweeney et.al (47), and created with BioRender.com.

The enrichment analysis indicates the most significant pathways and processes perturbed by 24 hours of DOX treatment. DEGs were mainly enriched in canonical pathways related to oxidative stress, apoptosis, development, and DNA damage (Figure 15A), and process networks related to all phases of the cell cycle (S-phase, Mitosis, G2-M, G1-S), DNA damage checkpoints, developmental processes, proteolysis, cytoskeleton, and cell adhesion (Figure 15B).

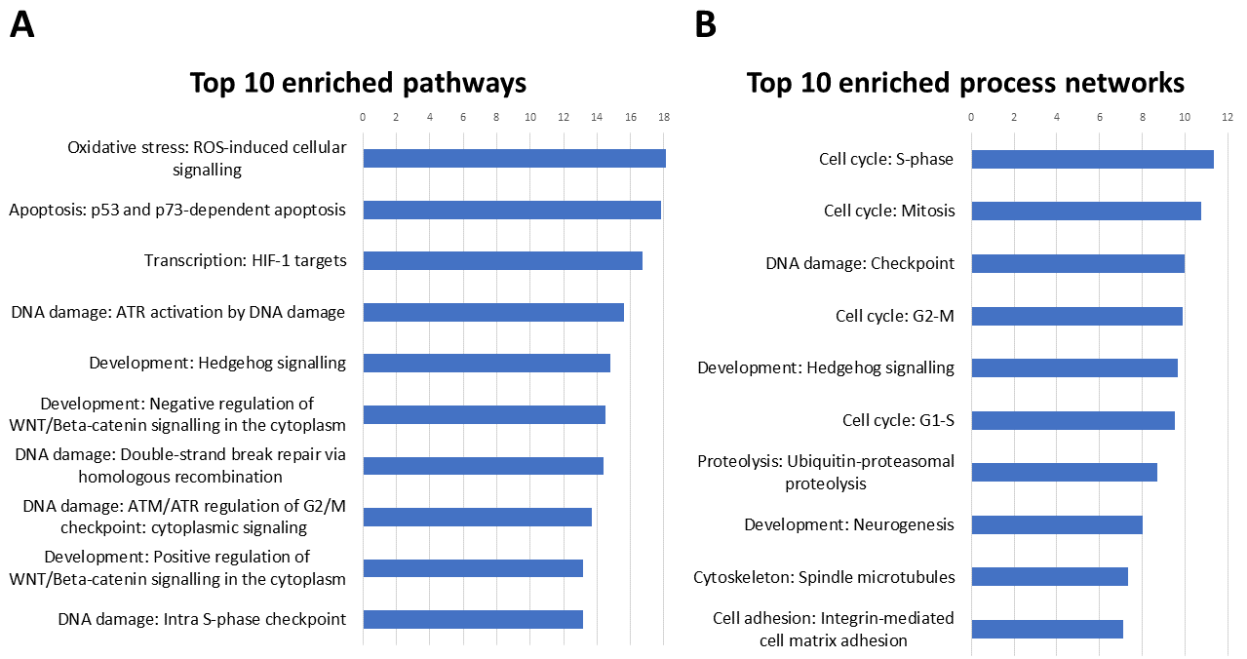

Figure 15: Top 10 enriched Metacore pathways and process networks

*AC16 CMs exposed to DOX (5μM) for 24 hours displayed DEGs enriched in pathways **(A)** related to oxidative stress, apoptosis, DNA damage and development, and in process networks **(B)** related to cell cycle, DNA damage, development, proteolysis, cytoskeleton, and cell adhesion. The histograms are adapted from the Metacore enrichment analysis results. Bars indicate -log(p-value). Pathway and process names are ranked according to lowest p-value from top to bottom. ATM: Ataxia telangiectasia mutated, ATR: Ataxia telangiectasia and Rad3 related, DEG: Differentially expressed gene, DOX: Doxorubicin, DNA: Deoxyribonucleic acid, HIF: Hypoxia inducible factor, ROS: Reactive oxygen species.*

4.3.1 DOX Induces Cell Death, Oxidative stress, and Inflammation

Oxidative stress: ROS-induced cellular signalling (-log(p-value) = 18.1) and *Transcription: Hypoxia inducible factor (HIF)-targets* (-log(p-value) = 16.7) were significantly enriched pathways, indicating presence of ROS-induced oxidative stress and cellular responses to a hypoxic environment, respectively. Upregulated HIF-induced transcripts were involved in fibrosis, extracellular matrix remodelling, angiogenesis, and stem cell maintenance (Appendix V). In the latter, the embryonic genes SRY-Box Transcription Factor 2 (SOX2), NANOG and Octamer-Binding Protein 3/4 (Oct-3/4) was significantly upregulated. The pathway map of *ROS-induced cellular signalling (Appendix III)* indicates upregulation of the inflammatory mediators IL6, IL8 and TNFα, and that apoptosis participants (NOXA, Bax, Bak, p21, cytochrome C, NF-κB) are differentially expressed. Enrichment of DEGs in *Apoptosis: p53 and p73-dependet apoptosis* (-log(p-value) =

17.8) (Appendix IV) further indicate apoptosis activation. DEGs involved in this pathway participates in the extrinsic (DR4, DR5, FasR, TRAIL) and intrinsic (Bax, Bak, Bcl-XL, Akt (PKB), Bim, Bik, NOXA) pathway of apoptosis. Together, this indicates altered transcription of genes involved in processes related to oxidative stress, cell death and inflammation.

4.3.2 DOX Alters The DDR

Both enriched pathways and process networks showed alterations in the cell cycle and DDR. DEGs were enriched in process networks related to DNA damage checkpoints, and pathways related to DS DNA break repair (*Double-strand break repair via homologous recombination* (-log(p-value) = 14.4) and the commonly activated DDR pathways *ATR activation by DNA damage* (-log(p-value) = 15.6) and *ATM/ATR regulation of G2/M checkpoint* (-log(p-value) = 13.7) (Figure 15). The G2/M checkpoint serves to prevent cells from entering mitosis upon DNA damage (48), while the enriched *Intra S-phase checkpoint* (-log(p-value) = 13.2) is activated to ensure genomic integrity prior to replication (49). Brca1 activation is involved in both checkpoints (48).

The majority of DEGs enriched in DNA damage pathways and processes were downregulated. This included the checkpoint kinase ATR and its downstream targets Chk1, Chk2 and MRN-complex members (19), and the important cell cycle regulators Brca1 and Brca2 (Appendix VI). These data indicate that transcription of several DDR participants and cell cycle regulators are shut down within 24 hours of DOX treatment. The few upregulated genes included histones, which serves important functions in chromatin remodelling, cyclins important for cell cycle progression, and the transcription factors ATF3 and c-Myc. The former transcription factor induces inflammatory responses, while the latter is a proto-oncogene with various functions.

4.3.3 DOX Activates Embryonic Pathways

DEGs were enriched in the embryonic pathway and process network of *Hedgehog-signalling* (-log(p-value) = 14.8) (Figure 15). Key participants in the Hedgehog-signalling pathway (SHH, GLI1, PTCH1, PTCH2, Smoothened) were significantly upregulated (Appendix VI). DEGs were also

enriched in *Positive regulation of Wnt/Beta-catenin signalling in the cytoplasm* (-log(p-value) = 13.2). Central pathway participants (Wnt, Frizzled, TCF/LEF1) were significantly upregulated, but contemporary enrichment of *Negative regulation of WNT/Beta-catenin signalling in the cytoplasm* (-log(p-value) = 14.5) indicate activation of a negative feedback mechanism. Hedgehog- and Wnt-signalling are evolutionary conserved pathways, important for normal embryonic development and adult tissue homeostasis (50-52).

4.4 Enrichment Analysis - Most Relevant Networks

The unique networks identified in the enrichment analysis indicate potentially important mediators and interactions involved in DOX responses. The networks were mainly enriched in GO processes related to development, inflammation, and cell growth (Table 1). The core genes of the highest ranked network included the transcription factors Krüppel like factor 4 (KLF4), Oct-3/4, SOX2, NANOG and Caudal Type Homeobox 2 (CDX2), and was enriched in GO processes related to embryonic development and cell fate commitment. KLF4 appeared as a hub for several transcripts in this network (Figure 16). Network 2 (Appendix VII) included the core genes TNF receptor associated factor (TRAF) 6, I-Kappa-B Kinase-Alpha (IKK-alpha), TLR4, I-kB and Interferon Regulatory Factor 7 (IRF7), and enriched GO processes was associated with inflammatory responses related to NFκB, IL1 and PRRs (Table 3). Network 3 (Appendix VIII) included the core genes SHC adaptor protein 1 (Shc), G protein alpha i-family, SOS Ras/Rac guanine nucleotide exchange factor 1 (SOS), phospholipase C beta 3 (PLC beta3), mitogen-activated protein kinase kinase 1 (MEK1(MAP2K1)), and the enriched GO processes were associated with cell surface receptor signalling, cellular response to growth factors and organic substances, and proliferation.

Table 1: The most relevant networks

Identified DEGs in AC16 CMs exposed to DOX (5μM) for 24 hours was involved in three unique networks. The most significant network (Network 1) included the core genes KLF4, Oct-3/4, SOX2, NANOG and CDX2. Dominant GO processes of this network related to embryonic development and cell fate commitment. Network 2 included the core genes TRAF6, IKK-alpha, TLR4, I-kB, IRF7, and GO processes associated with inflammatory responses involving NFκB, interleukin 1 and pattern recognition receptors. Network 3 included the core genes Shc, G protein alpha i family, SOS, PLC beta3, MEK1(MAP2K1), and was associated with the GO processes cell surface receptor signalling pathway, cellular response to growth factor stimulus, cellular response to organic substance, response to growth factor, and regulation of cell population proliferation. The networks are presented with size (number of nodes), targets (number of objects from the uploaded gene set), pathway fragments (the number of canonical pathway fragments included in the network) and p-value. CDX2: Caudal Type Homeobox 2, DEG: Differentially expressed gene, DOX: Doxorubicin, GO: Gene ontology, IKK-alpha: I-Kappa-B Kinase-Alpha, I-kB, IRF7: Interferon Regulatory Factor 7, KLF4: Krüppel like factor 4, MEK1(MAP2K1): mitogen-activated protein kinase kinase 1, Oct-3/4: Octamer-binding protein-3/4, PLC-beta3: phospholipase C beta 3, Shc: SHC adaptor protein 1, SOS: SOS Ras/Rac guanine nucleotide exchange factor 1, SOX2: SRY-Box Transcription Factor 2, TLR4: Toll-like receptor 4, TRAF6: TNF Receptor Associated Factor 6.

Most relevant networks

Name	**Network 1**	**Network 2**	**Network 3**
Core genes in network	KLF4, Oct-3/4, SOX2, NANOG, CDX2	TRAF6, IKK-alpha, TLR4, I-kB, IRF7	Shc, G-protein alpha-i family, SOS, PLC-beta3, MEK1(MAP2K1)
GO Processes	cell fate commitment (57.9%), cell fate commitment involved in formation of primary germ layer (36.8%), gastrulation (52.6%), formation of primary germ layer (47.4%), embryonic morphogenesis (63.2%)	pattern recognition receptor signalling pathway (69.6%), I-kappaB kinase/NF-kappaB signalling (56.5%), toll-like receptor signalling pathway (58.7%), cellular response to interleukin-1 (63.0%), positive regulation of NF-kappaB transcription factor activity (58.7%),	cell surface receptor signalling pathway (81.4%), cellular response to growth factor stimulus (52.5%), cellular response to organic substance (81.4%), response to growth factor (52.5%), regulation of cell population proliferation (71.2%)
Size	50	50	65
Target	47	29	39
Pathway fragments	27	15	9
P-value	$7.14e^{-65}$	$2.10e^{-29}$	$3.01e^{-40}$

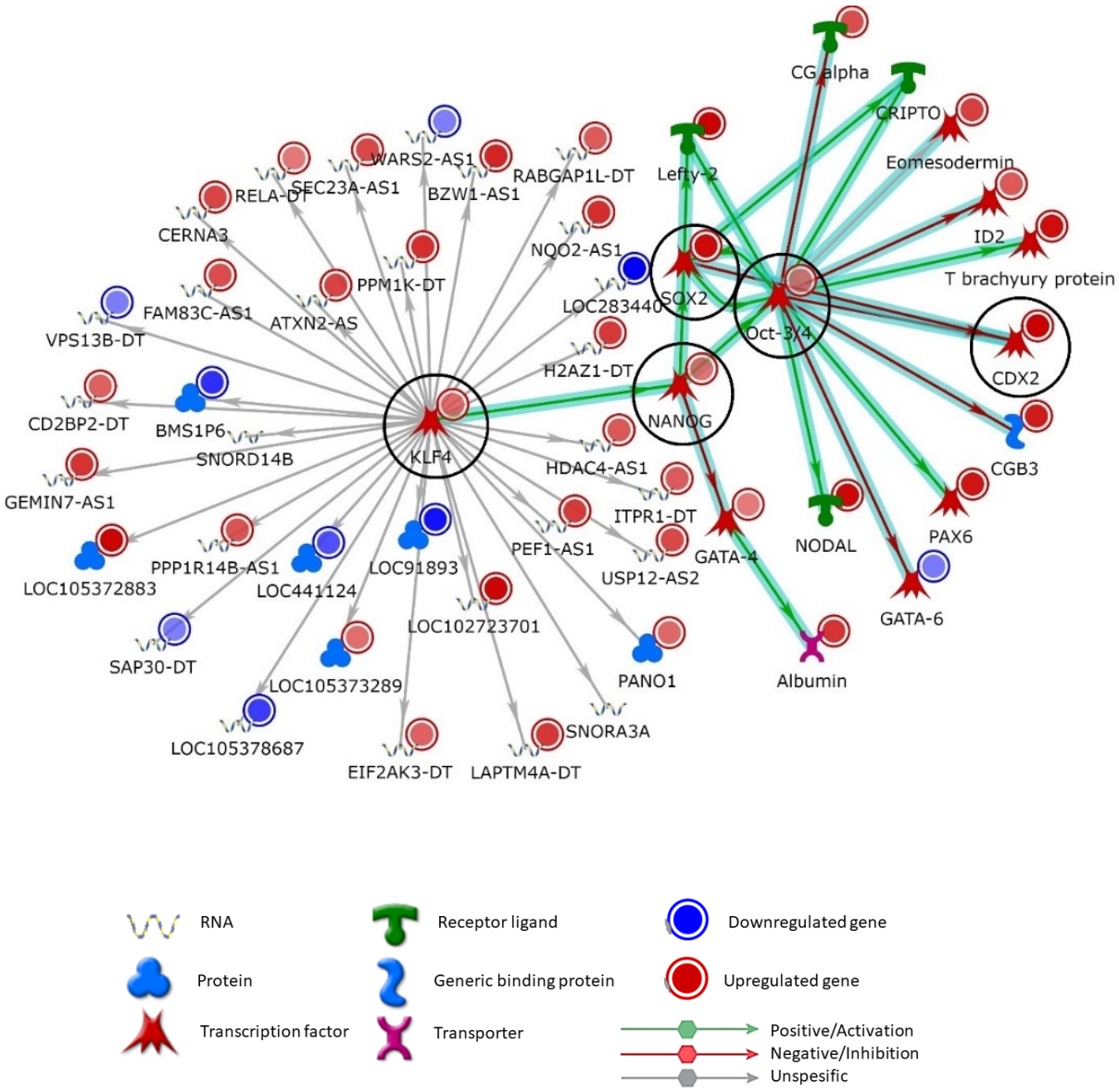

Figure 16: The most significant network

The most significant network (Network1) includes the core genes KLF4, Oct-3/4, SOX2, NANOG and CDX2 (encircled in black), and associated downstream targets. KLF4 was identified as a hub gene in the network. Enriched GO processes for the network was related to embryonic development and cell fate commitment. Arrows with thick cyan lines indicate fragments of canonical pathways. Green arrows indicate activation, while red arrows indicate inhibition. Upregulated genes (positive log2FC) are marked with red circles, downregulated genes (negative log2FC) are marked with blue circles. The brightness of the colour (red and blue) increases with increased Log2FC-value (positive and negative direction). Log2FC for network objects in Network 1 range from 7.3 (Lefty-2) to -3.6 (LOC283440). CDX2: Caudal Type Homeobox 2, FC: Fold change, GO: Gene ontology, Oct-3/4: Octamer-Binding Protein 3/4, SOX2: SRY-Box Transcription Factor 2.

5 Discussion

Increased understanding of the mechanisms contributing to DOX-induced cardiotoxicity is necessary to reduce morbidity and mortality among cancer survivors. The present study aimed to investigate the effect of DOX on cell death in AC16 CMs, and to explore the transcriptional changes following DOX treatment. The main findings include previously discussed pathological mechanisms, such as apoptosis, oxidative stress, inflammation, and DNA damage, but also less explored and novel pathways and processes related to development.

5.1 Cell Death

The great increase in LDH release from DOX-treated AC16 CMs provide evidence for increased acute cell death, an observation done in numerous studies (40, 53, 54). The differences in caspase 3/7 activity imply that a significant amount of cell death is caused by apoptosis. Further, the enrichment analysis showed DEGs to be enriched in pathways related to p53/p73-dependent cell death, suggesting that these contribute to the observed apoptosis. P53 is an established activator of the intrinsic pathway of apoptosis and activation of this pathway in response to DOX is observed in several studies (55-57). Even though the expression of pro-apoptotic mediators were significantly upregulated (Bik, Bim, NOXA), the expression of the apoptosis inducers Bax and Bak were significantly downregulated. This is somewhat surprising considering the central role of Bax and Bak in the induction of apoptosis. However, the current understanding is that Bax and Bak activation occurs through induction of conformational changes in the inactive protein (58). Therefore, it is a reasonable comprehension that the intrinsic pathway of apoptosis is activated in response to DOX, despite the decreased gene expression of Bak and Bax.

The p53 protein has also been linked to the extrinsic pathway of apoptosis through p53-dependet transcriptional activation of death receptor genes (59). Death receptors (DR4, DR5, FasR) were significantly upregulated in our gene set, an observation also recently reported at both mRNA and protein levels in human-induced pluripotent stem cell CMs (2, 47). Furthermore, p53 has been implicated as an important regulator of the DOX-response *in silico (47),* and to promote

cardiac mitochondrial dysfunction in mouse models exposed to DOX (60). Both cardiotoxic and cardioprotective effects have been described, and the outcome seem to depend on dose and duration of DOX treatment (21). It should be mentioned that the gene expression of p53 itself was not significantly altered in our analysis. However, this is in accordance with previous observations reporting DNA damage-induced p53-activation to occur independent of increasing its transcription (61). Taken together, our data therefore suggest a role of p53 in DOX-induced cardiotoxicity.

5.2 Oxidative Stress and Inflammation

The most significantly enriched pathway was *Oxidative stress: ROS-induced cellular signalling*, thereby giving evidence for significant ROS generation. The general upregulation of HIF-induced transcripts further supports the presence of oxidative stress. ROS generation has been recognized as a central aspect of DOX-induced cardiotoxicity for years (8), and the mitochondria is the major cellular ROS generator (62). Furthermore, DOX have shown to accumulate in the mitochondria (63), making its actions especially interesting in the highly metabolic heart. However, it has been questioned whether ROS accumulation is a cause or consequence of cardiotoxicity (64). Zhang et. al suggests that excessive ROS generation is a result of transcriptional changes caused by DOX (65), while a recent study by Helal et.al supports the view that redox cycling of DOX cause ROS-induced ROS-release (66). Despite the different views on ROS' role in cardiotoxicity, it is evident that ROS accumulation cause oxidative stress and subsequent inflammation, two conditions that are closely associated with development of heart failure (67).

DEGs included in the pathway of *ROS-induced cellular signalling* were related to inflammation, hypoxia, and cell death. Furthermore, the enriched processes of Network 2 (Table 1) give indications of IL1 activation, transcription of NFκB targets and alterations in the TLR-signalling pathway. Cell damage and necrotic cell death cause release of DAMPs. Further, DAMPs binds to PRRs, such as TLR2 and TLR4, which has been extensively studied in the heart (34). TLR2 and TLR4 was included in Network 2, where the former was significantly upregulated, and the latter was

significantly downregulated. Ma et.al (68) also observed distinct roles of TLR2 and TLR4 in their study of DOX-induced cardiomyopathy in mice. They found that inhibition of TLR2 led to reduction of left ventricle dysfunction and fibrosis, while inhibition of TLR4 exacerbated cardiac damage and inflammation, thereby suggesting a damaging role of TLR2, and a beneficial role of TLR4 in DOX-induced cardiotoxicity (68). However, the latter interpretation was contradicted by Riad et.al (69) who found that knock-out of TLR4 attenuated DOX-induced cardiomyopathy through reduction of oxidative stress, inflammation and apoptosis (69). Nevertheless, upregulation of TLR's downstream pro-inflammatory target genes IL6, IL8 and TNFα in our gene set gives evidence for an ongoing inflammatory response.

Sustained release of the abovementioned pro-inflammatory cytokines leads to recruitment of immune cells, causing chronic inflammation, remodelling of cardiac tissue and eventually development of heart failure (35, 67). Furthermore, TNFα and IL6 has shown to negatively affect the contractility of CMs in cell culture and animal models (35). TNFα has also shown increased expression in heart failure patients, thereby indicating an important link (70, 71). However, treatment with TNFα-antagonists have not shown clinically relevant effects, thereby questioning the direct effects of this mediator in heart failure development (72).

Both acute and progressive cell death is associated with development of cardiovascular diseases, such as heart failure (25). Due to the heart's limited ability to regenerate, even low rates of apoptosis and myocardial damage is detrimental (25). Previous observations prove unambiguous clues that cell death is evident in the hours and days following DOX treatment. However, it has been questioned whether acute cell death can explain the late onset of DOX-induced cardiomyopathy (16, 73). As previously mentioned, heart failure can manifest months, years or even decades after receiving DOX treatment. The late onset of heart failure indicates that DOX cause alterations in cellular functions that progress over time. Our RNA sequencing data point in several directions that can contribute to explain this late onset of disease. These include accumulation of genetic alterations, cellular senescence, and reactivation of embryonic pathways.

5.3 Altered DDR and Senescence

DEGs were highly enriched in pathways and processes related to the cell cycle, DNA damage and DNA repair, where the vast majority of genes were downregulated. Such downregulation of DNA repair genes has also been observed in DOX-treated human-induced pluripotent stem cell CMs (47, 74). This is surprising, considering that DOX is believed to induce DNA breaks in CMs through inhibition of TOP2β (65, 75), and that such DNA damage normally initiates the DDR through ATR- and ATM-pathway activation (30). Conversely, gene expression of several important mediators (ATR, Brca1, Chk1, Chk2, MRN-complex members) of these responses were significantly downregulated in our gene set. This is suggested to be part of the cascade of events following apoptosis initiation (23), however, it may also indicate a dysfunctional DDR. Impaired DNA repair cause accumulation of genetic alterations and may lead to aging-associated genomic instability (76). Premature aging has been described as a consequence of treatment with chemotherapeutics in several tissues (77), and after DOX treatment in rat CMs (78, 79). Therefore, our data may indicate that DOX accelerates genomic instability and aging in cardiac tissue, potentially explaining the early onset of heart failure in DOX-treated patients (79).

General downregulation of DNA damage repair genes has also been linked to cellular senescence (80). DOX have shown to induce senescence in human colon cancer cells *in vitro* (81) and in rat CMs *in vivo* (73). Stress-induced premature senescence can be induced by oxidative stress, prolonged DNA damage, and mitochondrial dysfunction (29, 30), all of which are discussed as potential contributors to DOX-induced cardiotoxicity. Furthermore, senescence-associated secretory phenotype CMs secretes TNFα, transforming growth factor (TGF)-β, IL6 and IL8, which are known promoters of cardiac inflammation and fibrosis (29). These inflammatory mediators were significantly upregulated in our gene set, and together this suggests a vicious combination of inflammation, senescence, and eventually premature cardiac tissue death in DOX-induced cardiotoxicity.

These interpretations are especially noteworthy regarding the increased susceptibility of DOX-induced cardiotoxicity in children and adolescents (3, 7). Similar to the associations made by McSweeney et.al (47), the immortalized AC16 CMs resemble immature CMs, in that they both

can proliferate. Mature CMs are thought to be terminally differentiated, having a turnover of less than 1% per year (36). Interestingly, Bergmann et.al (82) found that the highest postnatal turnover of CMs occurs within the first 10 years of age. Our data indicate that DOX induce transient or prolonged dysfunction to the DNA damage repair system in CMs that still have capacity to divide. Further, this might reduce the CMs ability to prevent proliferation of damaged cells in the still maturing heart. This may form an unfavourable basis for normal tissue maturation, making the heart more fragile to stressors in the future (3). Together with senescence and premature cardiac aging, this may explain the observation that young cancer survivors develop progressive heart failure several years after treatment (4, 79).

5.4 KLF4 and Endothelial-to-Mesenchymal Transition (EndMT)

Several of the enriched pathways, processes and networks were related to development and embryogenesis. The network analysis identified KLF4 as a key hub in the most significant network, a transcription factor involved in proliferation, differentiation and apoptosis in various tissues (83). A role of KLF4 in cardiac tissue processes and DOX responses is also emerging, and in AC16 CMs isolated TNFα stimuli revealed enhancers enriched in motifs for KLF4 (84), thereby suggesting that KLF4 activation is downstream of the inflammatory mediator TNFα.

Zhou et.al have suggested a role of KLF4 in the determination of p53's effects in response to DOX in cancer cells and HeLa cells (85). They found that the gene expression level of KLF4 was significantly decreased after apoptotic dose levels of DOX (5 μM/L), and that this was necessary for p53-mediated apoptosis. Further, they found that cytostatic levels of DOX (0.5 μM/L) caused cell cycle arrest through activation of p21. In contrast, we observed increased gene expression levels of KLF4, decreased gene expression levels of p21 and indications of p53 activation in response to 5 μM/L DOX. These distinct observations can be attributed to differences in treatment duration or cell type. As stated by Zhou et.al (85), KLF4 shows drastic cell context specific functions, making interpretation across cell types and environments speculative. However, despite the distinct observations, there are indications of KLF4 involvement in response to DOX.

In CMs, KLF4 is found to be important in adaption to hypertensive stress (86), to be a transcriptional regulator of mitochondrial homeostasis and directly regulate transcription of genes involved in autophagy (87). This is interesting, considering the observation that DOX accumulates in the mitochondria (9), and the indications that DOX treatment perturbs autophagic processes and induce mitochondrial dysfunction in cardiac tissue (88, 89).

KLF4 is together with SOX2, Oct3/4 and c-Myc also known as the Yamanaka factors. These factors were significantly upregulated, and central members of Network 1. The Yamanaka factors can reprogram somatic cells, thereby inducing pluripotency (83). In osteosarcomas, Li et.al found that DOX induced cancer stem cells through activation of KLF4 (90). Furthermore, transient expression of the Yamanaka factors improved cardiac damage and function after myocardial infarction in mice (91). KLF4 and c-Myc have also shown to induce differentiation of cardiac mesenchymal progenitor cells into adipocytes (92). This suggests that DOX can induce reprogramming of CMs through activation of the Yamanaka factors, thereby substituting CM specific properties and functions.

Similar alterations are seen in the developmental process of EndMT, where endothelial cells gain traits similar to mesenchymal cells, such as myofibroblasts and smooth muscle cells (93). Interestingly, KLF4 has shown to induce EndMT in cerebral endothelial cells (94, 95). Furthermore, EndMT has recently emerged as a potential contributor in the pathogenesis of several CVDs, including cardiac fibrosis, cardiomyopathy, heart failure, and DOX-induced cardiotoxicity (96-99). Xu et.al suggest that activation of the NFκB pathway is associated with induction of EndMT following DOX treatment in rats, and that this pathway could be a potential therapeutic target to prevent DOX-induced cardiotoxicity (99).

Our finding that DEGs were enriched in processes and networks related to NFκB supports this proposal. Moreover, other suggested promoters of EndMT induction including hypoxia, oxidative stress, TGF-β, TLR2, and Hedgehog- and Wnt/βcatenin signalling (98, 100, 101), are also enriched in the present gene set. Even though EndMT do not occur in CMs itself during development (95), these findings may indicate that DOX-treated CMs affect other cell types to undergo EndMT.

5.5 Hedgehog- and Wnt/βcatenin-signalling

The enriched Hedgehog- and Wnt/βcatenin-signalling pathways are evolutionary conserved and hold fundamental functions in human embryogenesis. Hedgehog-signalling participates in regulation of tissue patterning and angiogenesis (102-104), while Wnt/βcatenin-signalling is critical for development of the conduction system, valves and vessels of the heart (50, 105). Interestingly, both pathways have shown to be regulated by the Yamanaka factors (106), further underpinning an important role of the identified Network 1 and its core genes in DOX-induced cardiotoxicity.

Wnt-signalling is latent in adult CMs (107), and its reactivation has been observed in hypertrophy and myocardial infarction, where it contributes to revascularization and tissue remodelling (107, 108). Our enrichment analysis presented ambiguous indications of Wnt/βcatenin-pathway activation, in that DEGs were enriched in both positive and negative regulation of Wnt/βcatenin-signalling in the cytoplasm. This may suggest contemporary activation of a negative feedback mechanism, and potential inhibition of Wnt/βcatenin-signalling effects. DOX-induced inhibition of Wnt/βcatenin-signalling has previously been reported to increase DOX-induced cardiotoxicity (109, 110), suggesting an important role of Wnt/βcatenin-signalling in response to DOX.

Previous studies suggest that Hedgehog-signalling remains activated in adult CMs, serving important functions in maintenance of coronary vessels (103, 111). Our analyses strongly indicate activation of this pathway in response to DOX. Transient activation of Hedgehog-signalling has showed to protect against reperfusion injuries (51) and to decrease fibrosis formation and apoptosis in myocardial ischemia models (103). In contrast, sustained Hedgehog-signalling is associated with several malignancies (112). Hedgehog-signalling has also been associated with increased recruitment of bone-marrow derived endothelial stem cells believed to contribute in myocardial repair (103). However, similar to the initial reparative effect of tissue remodelling, exaggerated proliferation of endothelial stem cells in myocardial tissue might be detrimental (104). Therefore, the potential protective role of Hedgehog-signalling in cardiac tissue might depend on timing and duration. Hedgehog-signalling have, to our knowledge, not been

previously described in DOX-induced cardiotoxicity, making this observation especially interesting and a potential subject for further investigations.

The ability to regenerate cardiac tissue has been proposed as a potential therapeutic approach to circumvent dysfunctional myocardium after cardiac tissue damage. To transiently reactivate embryonic processes, such as the Yamanaka factors or the Hedgehog- and Wnt/βcatenin-signalling pathways, has been suggested as possible opportunities (38, 50, 51, 91). The enrichment of these mediators in DOX-treated CMs insinuate that these processes are in fact activated in response to DOX, and that potential therapeutic agents should aim at regulating these responses, instead of activating them. Nevertheless, regenerative medicine is still on the marks, and several aspects of this therapeutic approach remains to be elucidated and assessed *in vivo* (38).

As summarized in figure 17, the effects of DOX treatment may include acute responses such as oxidative stress, inflammation, acute cell death, and altered DDR, as well as activation of developmental processes and induction of senescence. These findings support previous comprehensions that the causes of DOX-induced cardiotoxicity are complex and multifactorial (3).

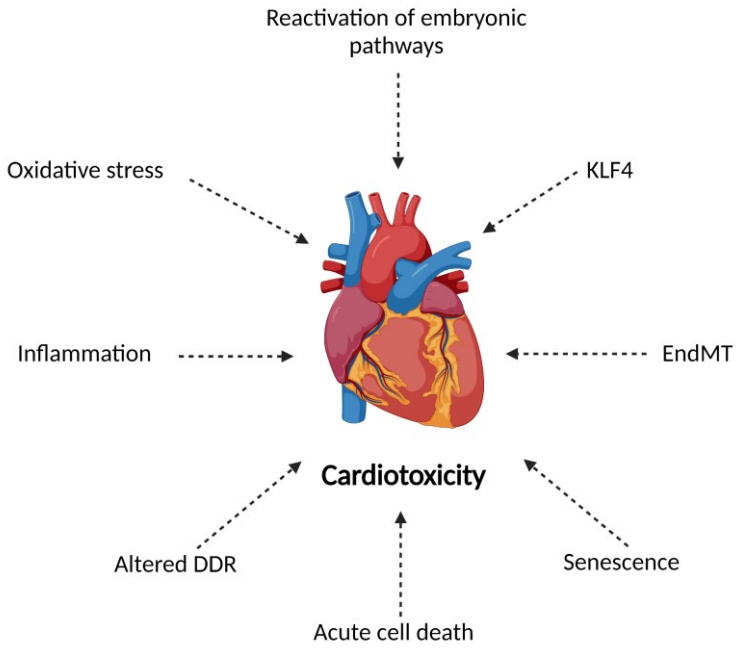

Figure 17: Proposed contributors to DOX-induced cardiotoxicity
Cell-based assays and enrichment analysis of transcriptomic data indicate involvement of oxidative stress, inflammation, altered DDR, acute cell death, senescence, EndMT, KLF4 and reactivation of embryonic pathways in the pathogenesis of DOX-induced cardiotoxicity. The figure was created with BioRender.com. DDR: DNA damage response, DOX: Doxorubicin, EndMT: Endothelial-to-mesenchymal transition, KLF4: Krüppel-like-factor 4.

6 Limitations and Future Perspectives

There are several limitations in this study. The cell line AC16 CMs was mainly chosen due its possession of human genome and its ability to produce relatively large amounts of biological sample, but also because it easily can be genetically modified. The original project aimed at exploring the protective effects of a specific protein in response to DOX treatment. Therefore, the cells were transfected with either EV or protein overexpression vector prior to assay and RNA sequencing. This may to some extents have affected the results of this study. However, we believe that the interfering effect of the transfection is minor, since it was performed in both experimental groups.

Cell culture arranges for close monitoring of the environment and high reproducibility and consistency of the data. However, there are limitations when it comes to using AC16 CMs as a

model for CM function, due to alterations of central functional properties, such as inadequate electric and contractile activity (39). This may influence the interpretation of the results. Furthermore, the lack of tissue heterogeneity will give an incomplete picture of the processes altered by DOX. Future studies should therefore evaluate the effect of DOX *in vivo* by studying isolated primary CMs, thereby enabling a more complete understanding of DOX exposure.

The chosen concentration of DOX and treatment duration were based on experiences and findings by Berg et.al (40). However, these variables are not representative for the actual therapeutic regimens used in cancer treatment. Thus, these findings are questionable in terms of therapeutic DOX dose effects. However, they still draw a picture of the cardiac pathways and processes affected by DOX.

The cell viability part of the multiplexed assay has shown to be influenced by high concentrations of DOX, due to its spontaneous emission of fluorescence (113). As such, the measured cell viability might be overestimated, thereby contributing to deviated interpretation. This problem could have been bypassed by measuring DOX-produced fluorescence prior to performing the assay. Despite this interfering factor, the high significance and consistent results nevertheless supports that DOX reduce cell viability.

The enrichment analysis identifies potentially important pathways and processes in the gene set. The cut-off $p < 0.01$ was set to only include highly significant DEGs. As a result, less significant DEGs that could still be relevant were excluded from the analysis. This may have affected the resulting pathways and processes of the analysis.

Bioinformatics approaches enables invaluable possibilities in terms of hypothesis generation. However, such findings will only be indications due to the potential influence of post-transcriptional and post-translational modifications. Therefore, the indications given in this study should be further explored through more targeted approaches, including proteomics analyses. Furthermore, it is not possible to distinguish between primary effects caused by DOX and secondary effects caused by processes initiated by DOX. Therefore, future studies should also be aimed at exploring the dynamic changes across a longer period.

7 Conclusion

In this project we assessed the effects of DOX treatment on cell death and the transcriptome in AC16 CMs. The findings of this study support the predominant role of ROS generation and DNA damage as major contributors to DOX-induced cardiotoxicity, but also sheds light on less explored participants, such as altered DDR, KLF4 and Wnt/βcatenin-signalling. Furthermore, the novel identification of Hedgehog-signalling activation is a curiosity that should be further assessed. As previously stated, DOX-induced cardiotoxicity is a complex and multifactorial condition. Accordingly, multiple aspects of the pathogenesis remain to be elucidated. Nevertheless, the findings of this study may contribute as a basis for future research aiming to combat DOX-induced cardiotoxicity in cancer survivors. Based on the initial aims of this project, the conclusions are that 24 hours of DOX treatment:

1. Increase cell death and apoptosis and decrease cell viability in AC16 CMs.
2. Induce significant transcriptional changes associated with apoptosis, oxidative stress, inflammatory responses, downregulation of DNA damage response genes, and reactivation of embryonic pathways. KLF4 appears as an important player in the DOX response, accompanied by the three additional Yamanaka factors, Wnt/βcatenin-signalling, and the novel curiosity of Hedgehog-signalling activation.

References

1. Masoudkabir F, Sarrafzadegan N, Gotay C, Ignaszewski A, Krahn AD, Davis MK, et al. Cardiovascular disease and cancer: Evidence for shared disease pathways and pharmacologic prevention. Atherosclerosis. 2017;263:343-51.
2. Zhao L, Zhang B. Doxorubicin induces cardiotoxicity through upregulation of death receptors mediated apoptosis in cardiomyocytes. Sci Rep. 2017;7:44735.
3. Carvalho FS, Burgeiro A, Garcia R, Moreno AJ, Carvalho RA, Oliveira PJ. Doxorubicin-induced cardiotoxicity: from bioenergetic failure and cell death to cardiomyopathy. Med Res Rev. 2014;34(1):106-35.
4. Angsutararux P, Luanpitpong S, Issaragrisil S. Chemotherapy-Induced Cardiotoxicity: Overview of the Roles of Oxidative Stress. Oxid Med Cell Longev. 2015;2015.
5. Herrmann J. Adverse cardiac effects of cancer therapies: cardiotoxicity and arrhythmia. Nat Rev Cardiol. 2020;17(8):474-502.
6. Weintraub RG, Semsarian C, Macdonald P. Dilated cardiomyopathy. Lancet. 2017;390(10092):400-14.
7. Wallace KB, Sardão VA, Oliveira PJ. Mitochondrial Determinants of Doxorubicin-Induced Cardiomyopathy. Circ Res. 2020;126(7):926-41.
8. Renu K, V GA, P BT, Arunachalam S. Molecular mechanism of doxorubicin-induced cardiomyopathy - An update. Eur J Pharmacol. 2018;818:241-53.
9. Wu BB, Leung KT, Poon EN. Mitochondrial-Targeted Therapy for Doxorubicin-Induced Cardiotoxicity. Int J Mol Sci. 2022;23(3).
10. Hausenloy DJ, Ng CT, Chong JH. Repeated Remote Ischemic Conditioning Protects Against Doxorubicin Cardiotoxicity: Never Too Much of a Good Thing. JACC CardioOncol. 2020;2(1):53-5.
11. McGowan JV, Chung R, Maulik A, Piotrowska I, Walker JM, Yellon DM. Anthracycline Chemotherapy and Cardiotoxicity. Cardiovasc Drugs Ther. 2017;31(1):63-75.
12. Zhang S, Liu XB, Bawa-Khalfe T, Lu LS, Lyu YL, Liu LF, et al. Identification of the molecular basis of doxorubicin-induced cardiotoxicity. Nat Med. 2012;18(11):1639-+.
13. Mei SB, Hong L, Cai XY, Xiao B, Zhang P, Shao L. Oxidative stress injury in doxorubicin-induced cardiotoxicity. Toxicol Lett. 2019;307:41-8.
14. Marin W, Marin D, Ao X, Liu Y. Mitochondria as a therapeutic target for cardiac ischemia-reperfusion injury (Review). Int J Mol Med. 2021;47(2):485-99.
15. Heusch G. Myocardial ischaemia-reperfusion injury and cardioprotection in perspective. Nature Reviews Cardiology. 2020;17(12):773-89.
16. Cappetta D, De Angelis A, Sapio L, Prezioso L, Illiano M, Quaini F, et al. Oxidative Stress and Cellular Response to Doxorubicin: A Common Factor in the Complex Milieu of Anthracycline Cardiotoxicity. Oxid Med Cell Longev. 2017;2017:1521020.
17. Surova O, Zhivotovsky B. Various modes of cell death induced by DNA damage. Oncogene. 2013;32(33):3789-97.
18. Roos WP, Kaina B. DNA damage-induced cell death: From specific DNA lesions to the DNA damage response and apoptosis. Cancer Lett. 2013;332(2):237-48.

19. Christmann M, Kaina B. Transcriptional regulation of human DNA repair genes following genotoxic stress: trigger mechanisms, inducible responses and genotoxic adaptation. Nucleic Acids Res. 2013;41(18):8403-20.
20. Shiloh Y, Ziv Y. The ATM protein kinase: regulating the cellular response to genotoxic stress, and more. Nature Reviews Molecular Cell Biology. 2013;14(4):197-210.
21. Men HB, Cai H, Cheng QL, Zhou WQ, Wang X, Huang S, et al. The regulatory roles of p53 in cardiovascular health and disease. Cell Mol Life Sci. 2021;78(5):2001-18.
22. Ma WJ, Wei SS, Zhang BK, Li WQ. Molecular Mechanisms of Cardiomyocyte Death in Drug-Induced Cardiotoxicity. Frontiers in Cell and Developmental Biology. 2020;8.
23. Ikeda S, Zablocki D, Sadoshima J. The role of autophagy in death of cardiomyocytes. J Mol Cell Cardiol. 2022;165:1-8.
24. Zhang YW, Shi JJ, Li YJ, Wei L. Cardiomyocyte death in doxorubicin-induced cardiotoxicity. Arch Immunol Ther Exp (Warsz). 2009;57(6):435-45.
25. Chiong M, Wang ZV, Pedrozo Z, Cao DJ, Troncoso R, Ibacache M, et al. Cardiomyocyte death: mechanisms and translational implications. Cell Death Dis. 2011;2(12):e244.
26. Teringova E, Tousek P. Apoptosis in ischemic heart disease. J Transl Med. 2017;15.
27. Del Re DP, Amgalan D, Linkermann A, Liu Q, Kitsis RN. Fundamental Mechanisms of Regulated Cell Death and Implications for Heart Disease. Physiol Rev. 2019;99(4):1765-817.
28. Yan C, Xu Z, Huang W. Cellular Senescence Affects Cardiac Regeneration and Repair in Ischemic Heart Disease. Aging Dis. 2021;12(2):552-69.
29. Chen MS, Lee RT, Garbern JC. Senescence mechanisms and targets in the heart. Cardiovasc Res. 2022;118(5):1173-87.
30. Hu C, Zhang X, Teng T, Ma ZG, Tang QZ. Cellular Senescence in Cardiovascular Diseases: A Systematic Review. Aging Dis. 2022;13(1):103-28.
31. Mehdizadeh M, Aguilar M, Thorin E, Ferbeyre G, Nattel S. The role of cellular senescence in cardiac disease: basic biology and clinical relevance. Nat Rev Cardiol. 2022;19(4):250-64.
32. Chao W. Toll-like receptor signaling: a critical modulator of cell survival and ischemic injury in the heart. Am J Physiol Heart Circ Physiol. 2009;296(1):H1-12.
33. Mann DL. Innate Immunity and the Failing Heart The Cytokine Hypothesis Revisited. Circ Res. 2015;116(7):1254-68.
34. Abdullah M, Berthiaume JM, Willis MS. Tumor necrosis factor receptor-associated factor 6 as a nuclear factor kappa B-modulating, therapeutic target in cardiovascular diseases: at the heart of it all. Translational Research. 2018;195:48-61.
35. Adamo L, Rocha-Resende C, Prabhu SD, Mann DL. Reappraising the role of inflammation in heart failure. Nature Reviews Cardiology. 2020;17(5):269-85.
36. Zhao MT, Ye S, Su J, Garg V. Cardiomyocyte Proliferation and Maturation: Two Sides of the Same Coin for Heart Regeneration. Front Cell Dev Biol. 2020;8:594226.
37. Kalyanaraman B. Teaching the basics of the mechanism of doxorubicin-induced cardiotoxicity: Have we been barking up the wrong tree? Redox Biol. 2020;29:101394.
38. Tenreiro MF, Louro AF, Alves PM, Serra M. Next generation of heart regenerative therapies: progress and promise of cardiac tissue engineering. NPJ Regen Med. 2021;6(1):30.

39. Davidson MM, Nesti C, Palenzuela L, Walker WF, Hernandez E, Protas L, et al. Novel cell lines derived from adult human ventricular cardiomyocytes. J Mol Cell Cardiol. 2005;39(1):133-47.
40. Berg PC, Hansson Å ML, Røsand Ø, Marwarha G, Høydal MA. Overexpression of Neuron-Derived Orphan Receptor 1 (NOR-1) Rescues Cardiomyocytes from Cell Death and Improves Viability after Doxorubicin Induced Stress. Biomedicines. 2021;9(9).
41. Kaja S, Payne AJ, Naumchuk Y, Koulen P. Quantification of Lactate Dehydrogenase for Cell Viability Testing Using Cell Lines and Primary Cultured Astrocytes. Curr Protoc Toxicol. 2017;72:2.26.1-2..10.
42. Kumar P, Nagarajan A, Uchil PD. Analysis of Cell Viability by the Lactate Dehydrogenase Assay. Cold Spring Harb Protoc. 2018;2018(6).
43. Riss TL, Moravec RA, Niles AL, Duellman S, Benink HA, Worzella TJ, et al. Cell Viability Assays. In: Markossian S, Grossman A, Brimacombe K, Arkin M, Auld D, Austin CP, et al., editors. Assay Guidance Manual. Bethesda (MD): Eli Lilly & Company and the National Center for Advancing Translational Sciences; 2004.
44. Gentleman RC, Carey VJ, Bates DM, Bolstad B, Dettling M, Dudoit S, et al. Bioconductor: open software development for computational biology and bioinformatics. Genome Biol. 2004;5(10):R80.
45. Anders S, Huber W. Differential expression analysis for sequence count data. Genome Biol. 2010;11(10):R106.
46. Love MI, Huber W, Anders S. Moderated estimation of fold change and dispersion for RNA-seq data with DESeq2. Genome Biol. 2014;15(12):550.
47. McSweeney KM, Bozza WP, Alterovitz WL, Zhang B. Transcriptomic profiling reveals p53 as a key regulator of doxorubicin-induced cardiotoxicity. Cell Death Discov. 2019;5:102.
48. Huen MS, Sy SM, Chen J. BRCA1 and its toolbox for the maintenance of genome integrity. Nat Rev Mol Cell Biol. 2010;11(2):138-48.
49. Iyer DR, Rhind N. The Intra-S Checkpoint Responses to DNA Damage. Genes (Basel). 2017;8(2).
50. Kahn M. Can we safely target the WNT pathway? Nat Rev Drug Discov. 2014;13(7):513-32.
51. Paulis L, Fauconnier J, Cazorla O, Thireau J, Soleti R, Vidal B, et al. Activation of Sonic hedgehog signaling in ventricular cardiomyocytes exerts cardioprotection against ischemia reperfusion injuries. Sci Rep. 2015;5:7983.
52. Kumar V, Vashishta M, Kong L, Wu X, Lu JJ, Guha C, et al. The Role of Notch, Hedgehog, and Wnt Signaling Pathways in the Resistance of Tumors to Anticancer Therapies. Front Cell Dev Biol. 2021;9:650772.
53. Zhong Z, Tian Y, Luo X, Zou J, Wu L, Tian J. Extracellular Vesicles Derived From Human Umbilical Cord Mesenchymal Stem Cells Protect Against DOX-Induced Heart Failure Through the miR-100-5p/NOX4 Pathway. Front Bioeng Biotechnol. 2021;9:703241.
54. Shi Y, Li F, Shen M, Sun C, Hao W, Wu C, et al. Luteolin Prevents Cardiac Dysfunction and Improves the Chemotherapeutic Efficacy of Doxorubicin in Breast Cancer. Front Cardiovasc Med. 2021;8:750186.
55. Childs AC, Phaneuf SL, Dirks AJ, Phillips T, Leeuwenburgh C. Doxorubicin treatment in vivo causes cytochrome C release and cardiomyocyte apoptosis, as well as increased

mitochondrial efficiency, superoxide dismutase activity, and Bcl-2:Bax ratio. Cancer Res. 2002;62(16):4592-8.
56. Jing X, Yang J, Jiang L, Chen J, Wang H. MicroRNA-29b Regulates the Mitochondria-Dependent Apoptotic Pathway by Targeting Bax in Doxorubicin Cardiotoxicity. Cell Physiol Biochem. 2018;48(2):692-704.
57. Sardão VA, Oliveira PJ, Holy J, Oliveira CR, Wallace KB. Doxorubicin-induced mitochondrial dysfunction is secondary to nuclear p53 activation in H9c2 cardiomyoblasts. Cancer Chemother Pharmacol. 2009;64(4):811-27.
58. Zhang J, Huang K, O'Neill KL, Pang X, Luo X. Bax/Bak activation in the absence of Bid, Bim, Puma, and p53. Cell Death Dis. 2016;7(6):e2266.
59. Aubrey BJ, Kelly GL, Janic A, Herold MJ, Strasser A. How does p53 induce apoptosis and how does this relate to p53-mediated tumour suppression? Cell Death Differ. 2018;25(1):104-13.
60. Hoshino A, Mita Y, Okawa Y, Ariyoshi M, Iwai-Kanai E, Ueyama T, et al. Cytosolic p53 inhibits Parkin-mediated mitophagy and promotes mitochondrial dysfunction in the mouse heart. Nat Commun. 2013;4:2308.
61. Kastan MB, Onyekwere O, Sidransky D, Vogelstein B, Craig RW. Participation of p53 protein in the cellular response to DNA damage. Cancer Res. 1991;51(23 Pt 1):6304-11.
62. Chen YR, Zweier JL. Cardiac Mitochondria and Reactive Oxygen Species Generation. Circ Res. 2014;114(3):524-37.
63. Ichikawa Y, Ghanefar M, Bayeva M, Wu RX, Khechaduri A, Prasad SVN, et al. Cardiotoxicity of doxorubicin is mediated through mitochondrial iron accumulation. J Clin Invest. 2014;124(2):617-30.
64. Varga ZV, Ferdinandy P, Liaudet L, Pacher P. Drug-induced mitochondrial dysfunction and cardiotoxicity. Am J Physiol Heart Circ Physiol. 2015;309(9):H1453-67.
65. Zhang S, Liu X, Bawa-Khalfe T, Lu LS, Lyu YL, Liu LF, et al. Identification of the molecular basis of doxorubicin-induced cardiotoxicity. Nat Med. 2012;18(11):1639-42.
66. Helal M, Alcorn J, Bandy B. Doxorubicin Cytotoxicity in Differentiated H9c2 Cardiomyocytes: Evidence for Acute Mitochondrial Superoxide Generation. Cardiovasc Toxicol. 2021;21(2):152-61.
67. Voigt A, Rahnefeld A, Kloetzel PM, Krüger E. Cytokine-induced oxidative stress in cardiac inflammation and heart failure-how the ubiquitin proteasome system targets this vicious cycle. Front Physiol. 2013;4:42.
68. Ma Y, Zhang X, Bao H, Mi S, Cai W, Yan H, et al. Toll-like receptor (TLR) 2 and TLR4 differentially regulate doxorubicin induced cardiomyopathy in mice. PLoS One. 2012;7(7):e40763.
69. Riad A, Bien S, Gratz M, Escher F, Westermann D, Heimesaat MM, et al. Toll-like receptor-4 deficiency attenuates doxorubicin-induced cardiomyopathy in mice. Eur J Heart Fail. 2008;10(3):233-43.
70. Torre-Amione G, Kapadia S, Lee J, Durand JB, Bies RD, Young JB, et al. Tumor necrosis factor-alpha and tumor necrosis factor receptors in the failing human heart. Circulation. 1996;93(4):704-11.

71. Doyama K, Fujiwara H, Fukumoto M, Tanaka M, Fujiwara Y, Oda T, et al. Tumour necrosis factor is expressed in cardiac tissues of patients with heart failure. Int J Cardiol. 1996;54(3):217-25.
72. Mann DL, McMurray JJ, Packer M, Swedberg K, Borer JS, Colucci WS, et al. Targeted anticytokine therapy in patients with chronic heart failure: results of the Randomized Etanercept Worldwide Evaluation (RENEWAL). Circulation. 2004;109(13):1594-602.
73. Spallarossa P, Altieri P, Aloi C, Garibaldi S, Barisione C, Ghigliotti G, et al. Doxorubicin induces senescence or apoptosis in rat neonatal cardiomyocytes by regulating the expression levels of the telomere binding factors 1 and 2. Am J Physiol Heart Circ Physiol. 2009;297(6):H2169-81.
74. Reyes ME, Ma J, Grove ML, Ater JL, Morrison AC, Hildebrandt MAT. RNA sequence analysis of inducible pluripotent stem cell-derived cardiomyocytes reveals altered expression of DNA damage and cell cycle genes in response to doxorubicin. Toxicol Appl Pharmacol. 2018;356:44-53.
75. Henriksen PA. Anthracycline cardiotoxicity: an update on mechanisms, monitoring and prevention. Heart. 2018;104(12):971-7.
76. Li Z, Zhang W, Chen Y, Guo W, Zhang J, Tang H, et al. Impaired DNA double-strand break repair contributes to the age-associated rise of genomic instability in humans. Cell Death Differ. 2016;23(11):1765-77.
77. Lubberts S, Meijer C, Demaria M, Gietema JA. Early ageing after cytotoxic treatment for testicular cancer and cellular senescence: Time to act. Crit Rev Oncol Hematol. 2020;151:102963.
78. Maejima Y, Adachi S, Ito H, Hirao K, Isobe M. Induction of premature senescence in cardiomyocytes by doxorubicin as a novel mechanism of myocardial damage. Aging Cell. 2008;7(2):125-36.
79. Mitry MA, Laurent D, Keith BL, Sira E, Eisenberg CA, Eisenberg LM, et al. Accelerated cardiomyocyte senescence contributes to late-onset doxorubicin-induced cardiotoxicity. Am J Physiol Cell Physiol. 2020;318(2):C380-c91.
80. Collin G, Huna A, Warnier M, Flaman JM, Bernard D. Transcriptional repression of DNA repair genes is a hallmark and a cause of cellular senescence. Cell Death Dis. 2018;9(3):259.
81. Sliwinska MA, Mosieniak G, Wolanin K, Babik A, Piwocka K, Magalska A, et al. Induction of senescence with doxorubicin leads to increased genomic instability of HCT116 cells. Mech Ageing Dev. 2009;130(1-2):24-32.
82. Bergmann O, Zdunek S, Felker A, Salehpour M, Alkass K, Bernard S, et al. Dynamics of Cell Generation and Turnover in the Human Heart. Cell. 2015;161(7):1566-75.
83. McConnell BB, Yang VW. Mammalian Krüppel-like factors in health and diseases. Physiol Rev. 2010;90(4):1337-81.
84. Luo X, Chae MH, Krishnakumar R, Danko CG, Kraus WL. Dynamic reorganization of the AC16 cardiomyocyte transcriptome in response to TNF alpha signaling revealed by integrated genomic analyses. BMC Genomics. 2014;15.
85. Zhou Q, Hong Y, Zhan Q, Shen Y, Liu Z. Role for Kruppel-like factor 4 in determining the outcome of p53 response to DNA damage. Cancer Res. 2009;69(21):8284-92.

86. Liao X, Haldar SM, Lu Y, Jeyaraj D, Paruchuri K, Nahori M, et al. Krüppel-like factor 4 regulates pressure-induced cardiac hypertrophy. J Mol Cell Cardiol. 2010;49(2):334-8.
87. Liao X, Zhang R, Lu Y, Prosdocimo DA, Sangwung P, Zhang L, et al. Kruppel-like factor 4 is critical for transcriptional control of cardiac mitochondrial homeostasis. J Clin Invest. 2015;125(9):3461-76.
88. Abdullah CS, Alam S, Aishwarya R, Miriyala S, Bhuiyan MAN, Panchatcharam M, et al. Doxorubicin-induced cardiomyopathy associated with inhibition of autophagic degradation process and defects in mitochondrial respiration. Sci Rep. 2019;9(1):2002.
89. Bartlett JJ, Trivedi PC, Pulinilkunnil T. Autophagic dysregulation in doxorubicin cardiomyopathy. J Mol Cell Cardiol. 2017;104:1-8.
90. Li Y, Xian M, Yang B, Ying M, He Q. Inhibition of KLF4 by Statins Reverses Adriamycin-Induced Metastasis and Cancer Stemness in Osteosarcoma Cells. Stem Cell Reports. 2017;8(6):1617-29.
91. Chen Y, Lüttmann FF, Schoger E, Schöler HR, Zelarayán LC, Kim KP, et al. Reversible reprogramming of cardiomyocytes to a fetal state drives heart regeneration in mice. Science. 2021;373(6562):1537-40.
92. Kami D, Kitani T, Kawasaki T, Gojo S. Cardiac mesenchymal progenitors differentiate into adipocytes via Klf4 and c-Myc. Cell Death Dis. 2016;7(4):e2190.
93. Kovacic JC, Dimmeler S, Harvey RP, Finkel T, Aikawa E, Krenning G, et al. Endothelial to Mesenchymal Transition in Cardiovascular Disease: JACC State-of-the-Art Review. J Am Coll Cardiol. 2019;73(2):190-209.
94. Alvandi Z, Bischoff J. Endothelial-Mesenchymal Transition in Cardiovascular Disease. Arterioscler Thromb Vasc Biol. 2021;41(9):2357-69.
95. Dejana E, Hirschi KK, Simons M. The molecular basis of endothelial cell plasticity. Nat Commun. 2017;8:14361.
96. Zeisberg EM, Tarnavski O, Zeisberg M, Dorfman AL, McMullen JR, Gustafsson E, et al. Endothelial-to-mesenchymal transition contributes to cardiac fibrosis. Nat Med. 2007;13(8):952-61.
97. Feng B, Cao Y, Chen S, Chu X, Chu Y, Chakrabarti S. miR-200b Mediates Endothelial-to-Mesenchymal Transition in Diabetic Cardiomyopathy. Diabetes. 2016;65(3):768-79.
98. Choi KJ, Nam JK, Kim JH, Choi SH, Lee YJ. Endothelial-to-mesenchymal transition in anticancer therapy and normal tissue damage. Exp Mol Med. 2020;52(5):781-92.
99. Xu A, Deng F, Chen Y, Kong Y, Pan L, Liao Q, et al. NF-κB pathway activation during endothelial-to-mesenchymal transition in a rat model of doxorubicin-induced cardiotoxicity. Biomed Pharmacother. 2020;130:110525.
100. Zhang L, He J, Wang J, Liu J, Chen Z, Deng B, et al. Knockout RAGE alleviates cardiac fibrosis through repressing endothelial-to-mesenchymal transition (EndMT) mediated by autophagy. Cell Death Dis. 2021;12(5):470.
101. Lin K, Luo W, Yan J, Shen S, Shen Q, Wang J, et al. TLR2 regulates angiotensin II-induced vascular remodeling and EndMT through NF-κB signaling. Aging (Albany N Y). 2020;13(2):2553-74.
102. Foulquier S, Daskalopoulos EP, Lluri G, Hermans KCM, Deb A, Blankesteijn WM. WNT Signaling in Cardiac and Vascular Disease. Pharmacol Rev. 2018;70(1):68-141.

103. Kusano KF, Pola R, Murayama T, Curry C, Kawamoto A, Iwakura A, et al. Sonic hedgehog myocardial gene therapy: tissue repair through transient reconstitution of embryonic signaling. Nat Med. 2005;11(11):1197-204.
104. Bijlsma MF, Peppelenbosch MP, Spek CA. Hedgehog morphogen in cardiovascular disease. Circulation. 2006;114(18):1985-91.
105. Christidi E, Brunham LR. Regulated cell death pathways in doxorubicin-induced cardiotoxicity. Cell Death Dis. 2021;12(4).
106. Liu X, Huang J, Chen T, Wang Y, Xin S, Li J, et al. Yamanaka factors critically regulate the developmental signaling network in mouse embryonic stem cells. Cell Res. 2008;18(12):1177-89.
107. Dawson K, Aflaki M, Nattel S. Role of the Wnt-Frizzled system in cardiac pathophysiology: a rapidly developing, poorly understood area with enormous potential. J Physiol. 2013;591(6):1409-32.
108. Zhang Q, Wang L, Wang S, Cheng H, Xu L, Pei G, et al. Signaling pathways and targeted therapy for myocardial infarction. Signal Transduct Target Ther. 2022;7(1):78.
109. Cao YJ, Li JY, Wang PX, Lin ZR, Yu WJ, Zhang JG, et al. PKC-zeta Aggravates Doxorubicin-Induced Cardiotoxicity by Inhibiting Wnt/beta-Catenin Signaling. Front Pharmacol. 2022;13.
110. Liang LY, Tu YL, Lu J, Wang PX, Guo Z, Wang QQ, et al. Dkk1 exacerbates doxorubicin-induced cardiotoxicity by inhibiting the Wnt/beta-catenin signaling pathway. J Cell Sci. 2019;132(10).
111. Lavine KJ, Kovacs A, Ornitz DM. Hedgehog signaling is critical for maintenance of the adult coronary vasculature in mice. J Clin Invest. 2008;118(7):2404-14.
112. Pelullo M, Zema S, Nardozza F, Checquolo S, Screpanti I, Bellavia D. Wnt, Notch, and TGF-β Pathways Impinge on Hedgehog Signaling Complexity: An Open Window on Cancer. Front Genet. 2019;10:711.
113. Wesierska-Gadek J, Gueorguieva M, Ranftler C, Zerza-Schnitzhofer G. A new multiplex assay allowing simultaneous detection of the inhibition of cell proliferation and induction of cell death. J Cell Biochem. 2005;96(1):1-7.

Appendices

Appendix I

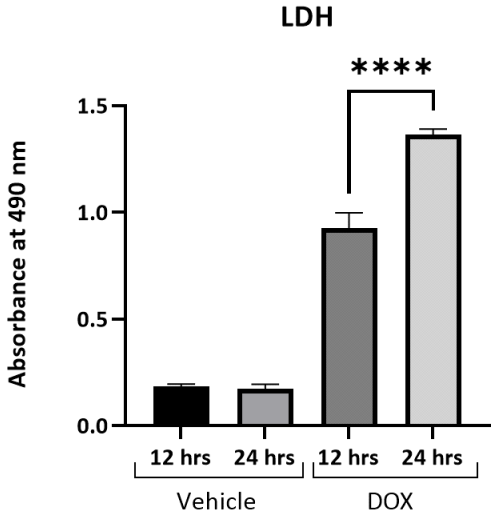

LDH activity after 12 vs 24 hours of DOX treatment

AC16 CMs were treated with DOX (5 µM) for 12 hours and 24 hours, respectively. There was a significantly higher LDH activity in the AC16 CMs treated for 24 hours, compared to the AC16 CMs treated for 12 hours. We wanted a robust change in LDH activity to be basis for the analyses, leading to the decision of 24 hours of treatment. Absorbance was measured at 490 nanometres. CM: Cardiomyocyte, DOX: Doxorubicin, LDH: Lactate dehydrogenase.

Appendix II

Concentration and purity control of isolated RNA samples

Samples 1-4 represents vehicle-treated AC16 CMs, while samples 5-8 represents DOX-treated AC16 CMs. Absorbance was measured at 260 nanometres and 230 nanometres, at which RNA and potential contaminants are absorbed, respectively. 260/230 and 260/280 ratio ~ 2 was considered pure. DOX: Doxorubicin, RNA: Ribonucleic acid.

Treatment	Samples	Concentration	260/230	260/280
Vehicle	1	1163.0 ng/µl	2.14	2.04
	2	758.1 ng/µl	2.10	2.06
	3	1235.9 ng/µl	2.11	2.01
	4	936.0 ng/µl	2.16	2.06
DOX	5	536.40 ng/µl	2.09	2.04
	6	570.13 ng/µl	2.15	2.06
	7	475.93 ng/µl	2.12	2.06
	8	551.00 ng/µl	1.98	2.06

Appendix III

Pathway map of Oxidative stress: ROS-induced cellular signalling

DEGs induced by 24 hours of DOX treatment were enriched in ROS-induced cellular signalling, and participated in processes related to apoptosis and inflammation, amongst others. The figure is generated by Metacore. DEG: Differentially expressed gene, DOX: Doxorubicin, GPCR: G-protein coupled receptor, ROS: Reactive oxygen species.

Appendix IV

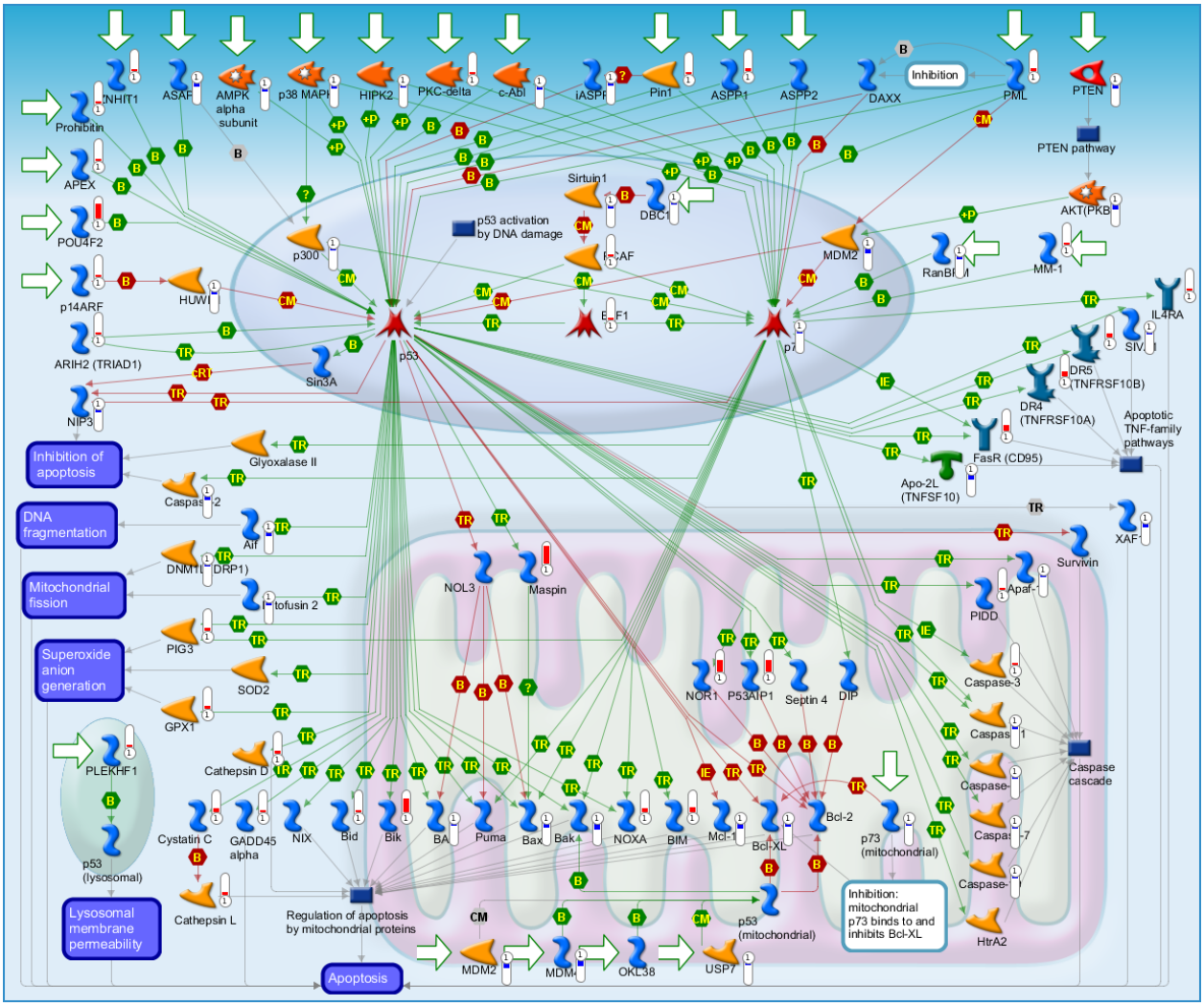

Pathway map of Apoptosis: P53/P73-induced apoptosis

DEGs induced by 24 hours of DOX treatment were enriched in P53/P73-induced apoptosis. DEGs involved in this pathway participates in the extrinsic (DR4, DR5, FasR, TRAIL) and intrinsic (Bax, Bak, Bcl-XL, Akt (PKB), Bim, Bik, NOXA) pathway of apoptosis. For legend explanations see Appendix III. The figure is generated by Metacore. DEG: Differentially expressed gene, DOX: Doxorubicin, DR: Death receptor, FasR: Fas-receptor, ROS: Reactive oxygen species, TRAIL: TNF-related apoptosis-inducing ligand.

Appendix V

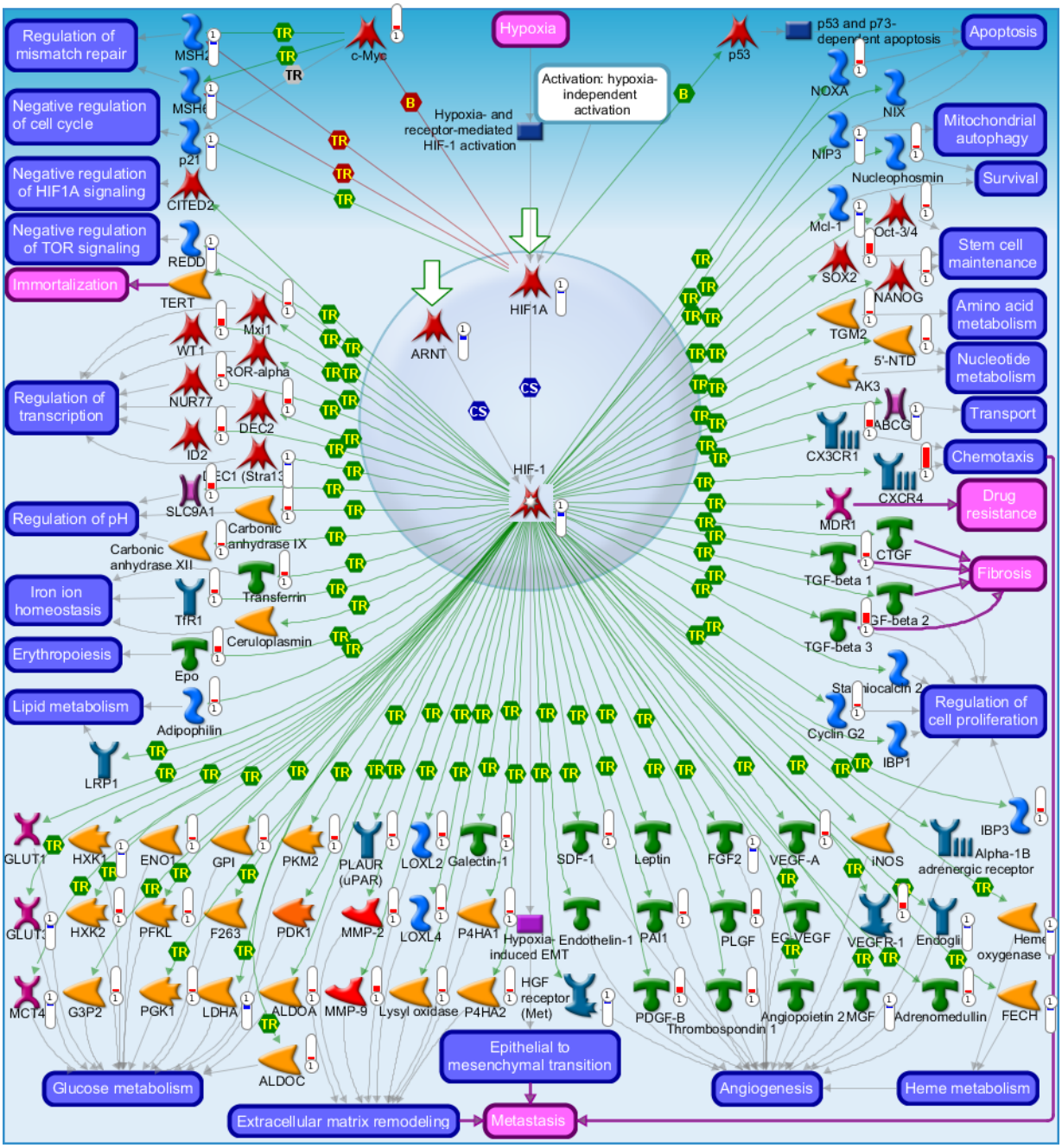

Pathway map of Transcription: HIF targets

DEGs induced by 24 hours of DOX treatment were enriched in HIF targets, and participated in processes related to fibrosis, extracellular matrix remodelling, angiogenesis, and stem cell maintenance, amongst others. For legend explanations see Appendix III. The figure is generated by Metacore. DEG: Differentially expressed gene, DOX: Doxorubicin, HIF: Hypoxia inducible factor, ROS: Reactive oxygen species.

Appendix VI

DEGs in the top 10 enriched pathways

The pathways included Oxidative stress: ROS-induced cellular signalling, Apoptosis: p53 and p73-dependent apoptosis, Transcription: HIF-1 targets, DNA damage: ATR activation by DNA damage, Development: Hedgehog signalling, Development: Negative regulation of WNT/Beta-catenin signalling in the cytoplasm, DNA damage: Double-strand break repair via homologous recombination DNA damage: ATM/ATR regulation of G2/M checkpoint: cytoplasmic signalling, Development: Positive regulation of WNT/Beta-catenin signalling in the cytoplasm DNA damage: Intra S-phase checkpoint when sorted by p-value. Only DEGs with log2FC > 1 were included. DEGs are reported with Metacore annotations in alphabetical order. DEG: Differentially expressed gene, FC: Fold change.

Oxidative stress: ROS-induced cellular signalling		**Apoptosis: p53 and p73-dependent apoptosis**	
Positive Log2FC > 1	*Negative Log2FC > 1*	*Positive Log2FC > 1*	*Negative Log2FC > 1*
Adrenomedullin	ACACA	ASPP1	Aif
Carbonic anhydrase IX	AKT(PKB)	Bik	AKT(PKB)
COX-2 (PTGS2)	AMPK alpha subunit	Bim	AMPK alpha subunit
Cyclin D1	Bak	Cathepsin D	Apo-2L(TNFSF10)
Cytochrome c	Bax	Cathepsin L	ASAP
EGLN3	c-Abl	Cystatin C	Bak
FTH1	Casein kinase II, alpha chains	DR4(TNFRSF10A)	Bax
FTL	Chk2	DR5(TNFRSF10B)	Bcl-XL
GPX1	Cyclin B1	FasR(CD95)	c-Abl
GSTP1	FIH-1	GPX1	Caspase-1
HES1	Heme oxygenase 1	Maspin	Caspase-2
HIF-prolyl hydroxylase	HIF1A	NOR1	HUWE1
IL-6	IKK-alpha	NOXA	iASPP
IL-8	MDM2	P53AIP1	Mcl-1
JNK(MAPK8-10)	mTOR	PIG3	MDM2
NALP3	NF-kB	PML	MDM4
NOTCH1 (NICD)	NIK(MAP3K14)	POU4F2	Mitofusin 2
NOXA	NRF2		p38 MAPK
PAI1	p21		PTEN
PAX5	p38 MAPK		RanBPM
PKC	p38alpha (MAPK14)		Sirtuin1
PLK3 (CNK)	PKA-reg (cAMP-dependent)		XAF1
TfR1	PRKD1		
Thioredoxin	PTEN		
TNF-alpha	RelA (p65 NF-kB subunit)		
VEGF-A	SAE2		
	SENP1		
	Sirtuin1		
	TXNIP (VDUP1)		

Transcription: HIF-1 targets		Development: Hedgehog signalling	
Positive Log2FC > 1	*Negative Log2FC > 1*	*Positive Log2FC > 1*	*Negative Log2FC > 1*
Adipophilin	ARNT	Adenylate cyclase	AKT(PKB)
Adrenomedullin	FGF2	ALPL	CARD7
Carbonic anhydrase IX	GLUT3	BMP2	CARD8
c-Myc	Heme oxygenase 1	BOC	Caspase-9
CX3CR1	HGF receptor (Met)	c-Fes	KIF3A
CXCR4	HIF-1	Collagen X	LGN
DEC2	HIF1A	Cyclin D1	Liprin-alpha1
Epo	HXK1	DHH	LKB1
G3P2	LDHA	E2F2	MED12
Galectin-1	Mcl-1	EGLN3	PI3K cat class IA
HXK2	MGF	FOXC1	PKA-reg
IBP3	MSH2	GLI-1	PLC-beta
ID2	MSH6	G-protein beta/gamma	PRMT5
LOXL2	p21	HNF3-beta	ROCK
LOXL4		Ihh	
Lysyl oxidase		Nkx2.2	
MMP-2		Nkx2.8	
MMP-9		N-Myc	
NANOG		PI3K reg class IA	
NOXA		PTCH1	
P4HA1		PTCH2	
PAI1		PTHrP	
PDGF-B		SHH	
PFKL		Smoothened	
PGK1		SOX14	
PKM2		SOX9	
PLAUR (uPAR)		TITF1	
PLGF			
SLC9A1			
SOX2			
TfR1			
TGF-beta 1			
TGF-beta 3			
TGM2			
Thrombospondin 1			
Transferrin			
VEGF-A			
VEGFR-1			
WT1			

DNA damage: ATM/ATR regulation of G2/M checkpoint: cytoplasmic signalling		DNA damage: Intra S-phase checkpoint	
Positive Log2FC > 1	*Negative Log2FC > 1*	*Positive Log2FC > 1*	*Negative Log2FC > 1*
Histone H3	14-3-3	ATF-3	ASF1A
	ATR	c-Myc	ASK (Dbf4)
	Aurora-A	Cyclin A	ATR
	Aurora-B	Histone H3	beta-TrCP
	beta-TrCP		BLM
	BORA		Brca1
	Brca1		BRIP1
	Brca1/Bard1		CDC18L (CDC6)
	c-Abl		CDC25A
	CDC25A		CDC7
	CDC25B		CDH1
	CDC25C		Chk1
	Chk1		Chk2
	Chk2		DTL (hCdt2)
	Cyclin B1		FANCD2
	DCK		FBXW11
	JAB1		HBOA
	JIK		Histone H2AX
	MARKK		HUWE1
	MEK6(MAP2K6)		MCM3
	MLCP (reg)		Mitotic cohesin complex
	Nek11		MRN complex
	p38 MAPK		NFBD1
	p38alpha (MAPK14)		Nibrin
	p38gamma (MAPK12)		p21
	PARN		p38 MAPK
	PLK1		p53BP1
	PP1-cat		PCNA
	PP2A regulatory		PP1-cat
	UBE2C		PP1-cat gamma
			RAD18
			Rad50
			RIF1
			RPA2
			Sirtuin1
			SMC3
			TLK1
			TOPBP1

DNA damage: ATR activation by DNA damage		DNA damage: Double-strand break repair via homologous recombination	
Positive Log2FC > 1	*Negative Log2FC > 1*	*Positive Log2FC > 1*	*Negative Log2FC > 1*
ATRIP	ATR	Histone H2A	BLM
EGLN3	Chk1	Histone H2B	Brca1
	CINP	Histone H4	Brca2
	FANCM	USP20 (VDU2)	BRD9
	Histone H2AX		BRG1
	HUWE1		BRIP1
	Kendrin		CCDC98 (Abraxas)
	LARG		DNA polymerase eta
	Microcephalin		DNA2
	MRN complex		EXO1
	MutYH		FANCM
	NEK1		FIGNL1
	NFBD1		Histone H2AX
	Nibrin		HROB
	NMP200		MCM9
	p53BP1		MRN complex
	PP5		NARF
	PRMT5		NEK1
	RAD17		NFBD1
	Rad50		Nibrin
	RBBP8 (CtIP)		NUCKS
	RPA2		p53BP1
	Sirtuin1		PALB2
	SNIP1		PIR51
	TLK1		PLK1
	TOPBP1TTI2		RAD18
			Rad51
			RAD51C
			Rad52
			RAD54B
			RBBP8 (CtIP)
			REV1
			RIF1
			RING1
			RMI2
			RNF168
			RNF20
			SFR1
			SMARCA5
			SMARCAD1
			SPIDR
			SWI5
			TOPBP1
			USP4
			WDHD1
			WRN
			ZGRF1

Development: Negative regulation of WNT/Beta-catenin signalling in the cytoplasm		Development: Positive regulation of WNT/Beta-catenin signalling in the cytoplasm	
Positive Log2FC > 1	*Negative Log2FC > 1*	*Positive Log2FC > 1*	*Negative Log2FC > 1*
A20	Ankyrin-G	Axin	14-3-3
Axin	beta-TrCP	Bcl-9	AKT(PKB)
Beclin 1	Casein kinase I alpha	COX-2 (PTGS2)	BIG1
Casein kinase I epsilon	c-Cbl	DACT1	BIG2
CXXC4	DAB2	Frizzled	Casein kinase II, alpha chains
Cyclin D1	Dsh	GSKIP	DOCK4
CYLD	FAF1	ITGB1	Dsh
DACT1	GSK3 alpha/beta	JNK(MAPK8-10)	FAK1
DACT3	HECTD1	NKD1	GSK3 alpha/beta
E-cadherin	HUWE1	RIPK4	HECTD1
Frizzled	Itch	SET7	Jouberin
G-protein beta/gamma	KLHL12	Tcf(Lef)	PKA-reg type II
KCTD1	LATS1	TGF-beta 1	PP1-cat
NKD1	Malin	TGIF	PPP2R2A
NOTCH1 receptor	NEDD4L	WNT	RNF146
PEG3	Nucleoredoxin		RNF220
RIPK4	PI3K cat class III (Vps34)		SMAD4
Tcf(Lef)	PKC-alpha		Tankyrases
WNT	PP1-cat		TBL1X
	Presenilin 1		Trabid
	RACK1		UBE2B
	SENP2		USP25
	STK3		USP47
	STK4		USP9X
	VHL		ZBED3
	WWP1		

Appendix VII

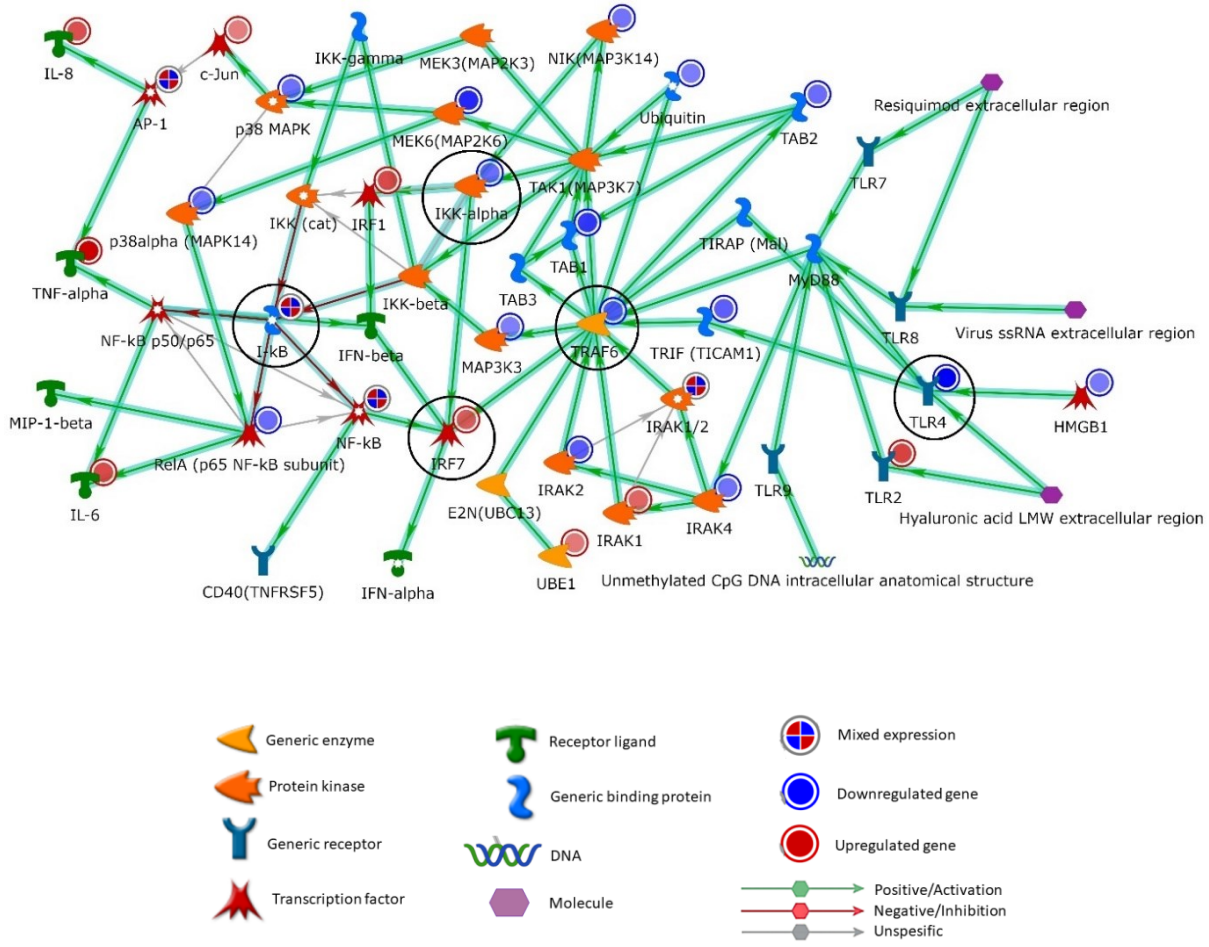

The second most significant network

Network 2 includes the core genes TRAF6, IKK-alpha, TLR4, I-kB and IRF7, and its interacting genes. Enriched GO processes of the network was associated with inflammatory responses involving NFκB, IL1 and PRRs. Arrows with thick cyan lines indicate fragments of canonical pathways. Core genes identified by the Metacore algorithm are encircled in black. Green arrows indicate activation, while red arrows indicate inhibition. Upregulated genes (positive log2FC) are marked with red circles, downregulated genes (negative log2FC) are marked with blue circles. The brightness of the colour (red and blue) increases with increased Log2FC-value (positive and negative direction). A combination of red and blue circles indicates mixed expression for the gene between multiple Metacore-tags for the same gene. Log2FC for network objects in Network 2 range from 6.0 (TNFα) to -5.1 (TLR4). FC: Fold change, GO: Gene ontology, IL: Interleukin, IRF7: Interferon Regulatory Factor 7, NFκB: Nuclear factor kappa B, PRR: Pattern recognition receptor, TLR4: Toll-like receptor 4, TNFα: Tumour necrosis factor α, TRAF6: TNF receptor associated factor 6.

Appendix VIII

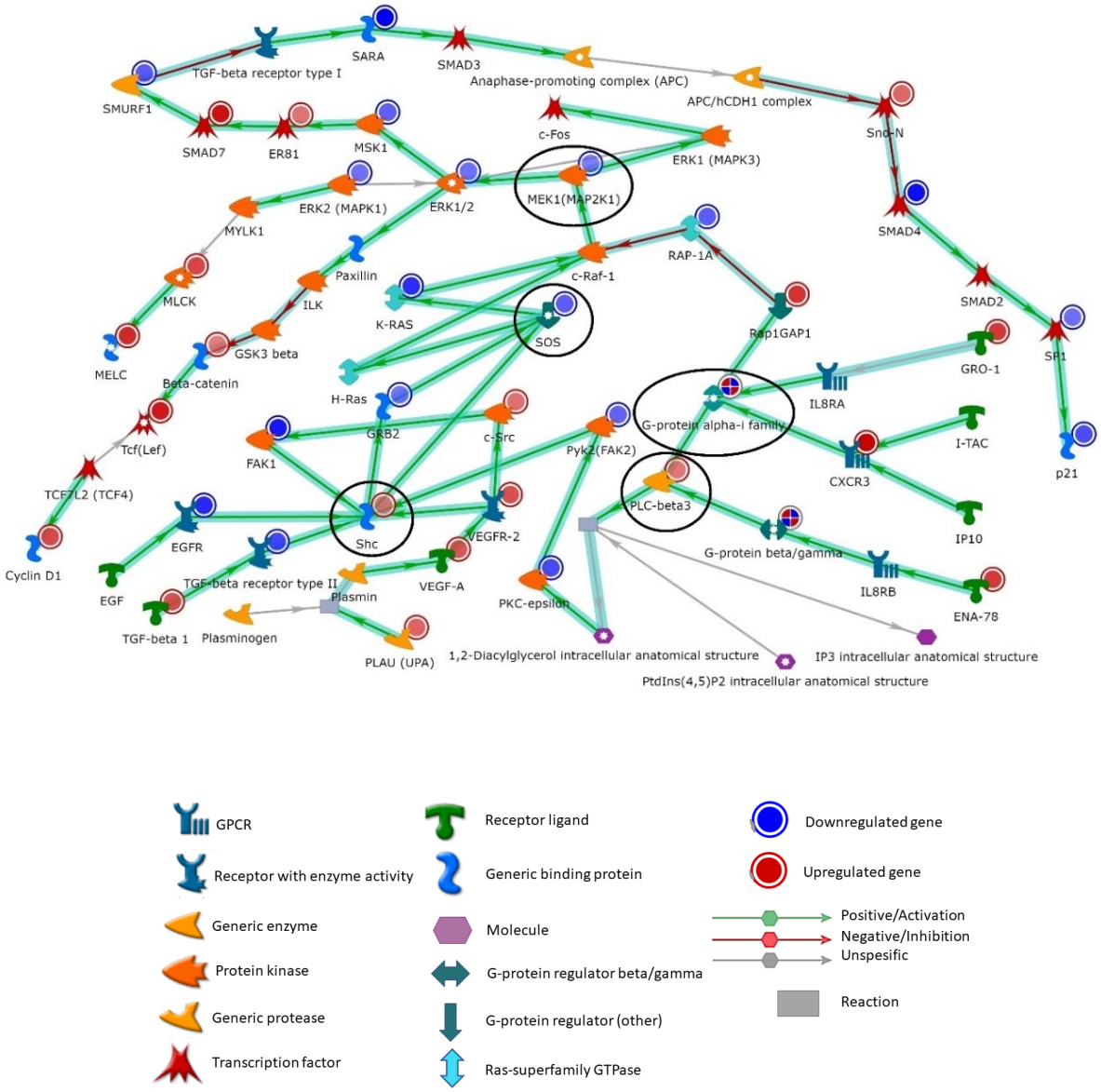

The third most significant network

Network 3 includes Shc, G protein alpha i family, SOS, PLC beta3, MEK1(MAP2K1), and its interacting genes. Enriched GO processes of the network included cell surface receptor signalling pathway, cellular response to growth factor stimulus, cellular response to organic substance, response to growth factor, and regulation of cell population proliferation. Arrows with thick cyan lines indicate fragments of canonical pathways. Core genes identified by the Metacore algorithm are encircled in black. Green arrows indicate activation, while red arrows indicate inhibition. Upregulated genes (positive log2FC) are marked with red circles, downregulated genes (negative log2FC) are marked with blue circles. The brightness of the colour (red and blue) increases with increased Log2FC-value (positive and negative direction). A combination of red and blue circles indicates mixed expression for the gene between multiple Metacore-tags for the same gene. Log2FC for network objects in Network 3 range from 4.5 (CXCR3) to -2.8 (SARA (ZFYV9)). CXCR3: C-X-C Motif Chemokine Receptor 3, FC: Fold change, GO: Gene ontology, MEK1(MAP2K1): mitogen-activated protein kinase kinase 1, PLC beta3: phospholipase C beta 3, Shc: SHC adaptor protein 1, SOS: SOS Ras/Rac guanine nucleotide exchange factor 1, ZFVY9: Zinc Finger FYVE-Type Containing 9.

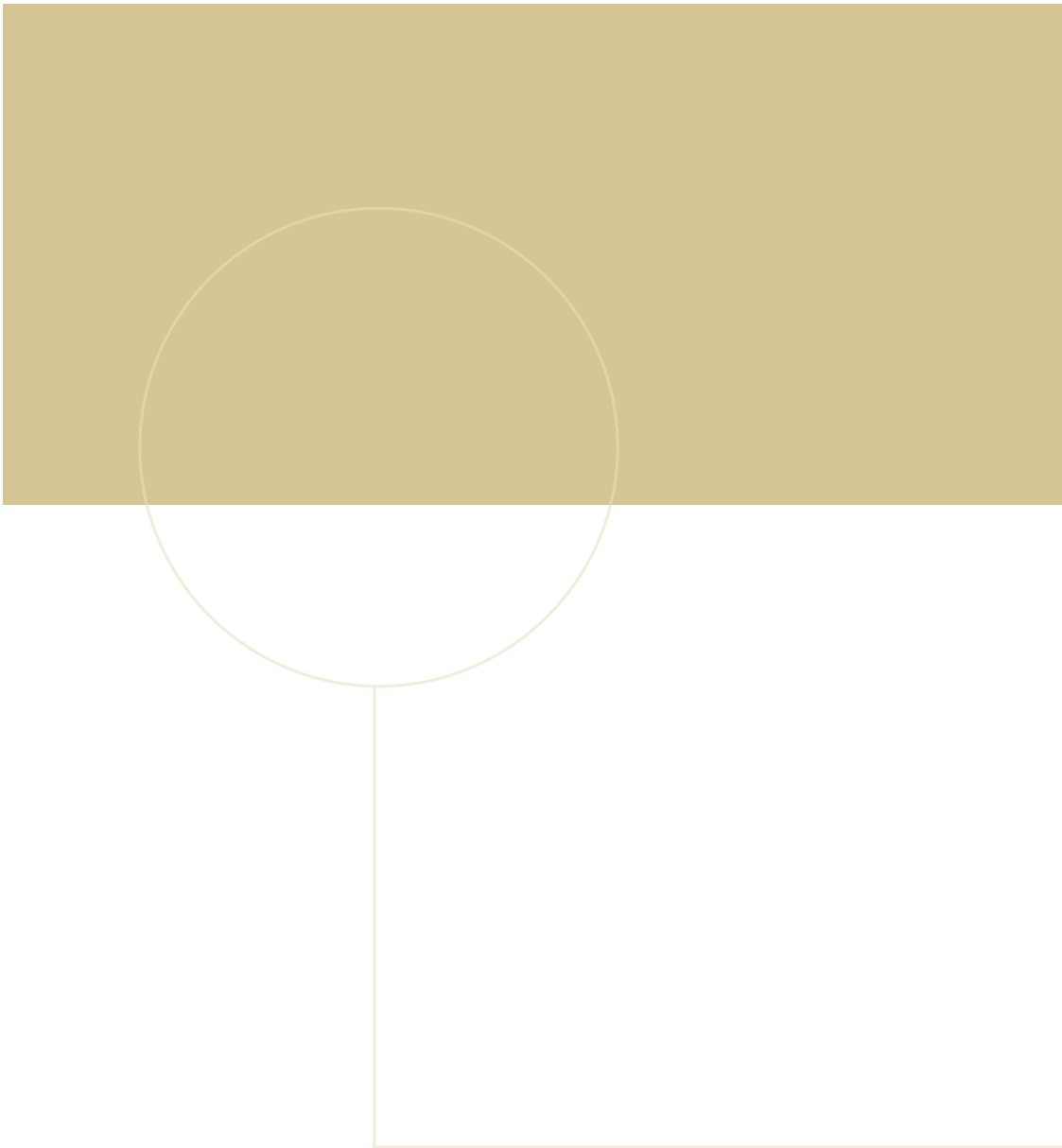

NTNU

Kunnskap for en bedre verden